

# Numerical study of the stabilisation of boundary-layer disturbances by finite amplitude streaks

Philipp Schlatter<sup>†\*</sup>, Enrico Deusebio<sup>†</sup>, Rick de Lange<sup>‡</sup>, Luca Brandt<sup>†</sup>

<sup>†</sup> Swedish e-Science Research Centre (SeRC)  
Linné FLOW Centre, KTH Mechanics  
Osquars Backe 18, SE-100 44 Stockholm, Sweden

<sup>‡</sup> TUE, Mechanical Engineering  
Den Dolech 2, NL-5612 AZ Eindhoven, The Netherlands

March 2, 2011

## Abstract

Well-resolved large-eddy simulations of passive control of the laminar-turbulent transition process in flat-plate boundary-layer flows are presented. A specific passive control mechanism is studied, namely the modulation of the laminar boundary-layer profile by a periodic array of steady boundary-layer streaks. This has been shown experimentally to stabilise the exponential growth of Tollmien-Schlichting (TS) waves and delay transition to turbulence. Here we examine the effect of the steady modulations on the amplification of different types of disturbances such as TS-waves, stochastic noise and free-stream turbulence. In our numerical simulations, the streaks are forced at the inflow as optimal solutions to the linear parabolic stability equations (PSE), whereas the additional disturbances are excited via volume forcing active within the computational domain. The simulation results show, in agreement with experimental and theoretical studies, significant damping of unstable two-dimensional TS-waves of various frequencies when introduced into a modulated base flow: The damping characteristics are mainly dependent on the streak amplitude. A new phenomenon is also identified which is characterised by the strong amplification via nonlinear interactions of the second spanwise harmonic of the streak when the streak amplitude is comparable to the TS amplitude. Furthermore, we demonstrate that control by streaks can be effective also in case of stochastic two-dimensional noise. However, as soon as a significant three-dimensionality is dominant, as in *e.g.* oblique or bypass transition, control by streaks leads often to premature transition. Visualisations of the flow fields are used to highlight the different vortical structures and their interactions that are relevant to the various transition scenarios and the corresponding control by streamwise streaks.

## 1 Introduction

The reduction and control of the viscous drag force exerted on thin bodies moving in a fluid is of great technical interest. Drag reduction can be achieved by delaying the onset of a turbulent flow as well as quenching turbulence itself. Several active and passive methods to reduce the drag associated to a turbulent flow and/or achieve a delay of laminar-turbulent transition in

---

\*Corresponding author: pschlatt@mech.kth.se

the boundary layer have been developed in the past. Due to the highly local nature of turbulent events and the rapid nature of the breakdown a sensor-less (open-loop) strategy may be preferable, since it prevents the necessity of large numbers of fast sensor/actuator combinations (recent progress in feedback control of boundary layer instabilities can be found in *e.g.* [1, 2]). Thus far, the success of the control strategies for boundary-layer flows is limited and for bypass transition, *i.e.* transition in boundary layers subject to high levels of external perturbations, none of the strategies has been successful.

Attention has been given to control via wall blowing/suction in the form of traveling waves. Du and Karniadakis [3] first showed drag reduction for control in the form of spanwise traveling waves in turbulent channel flow, actually implemented using volume forcing. These waves sustain streaky structures which are not optimal for transition or to sustain turbulence and could thus reduce the drag. More recently, Quadrio and coworkers [4, 5] examined the drag reduction in turbulent channel flow by wall actuation in the form of streamwise traveling waves of spanwise velocity perturbations. In these investigations a more feasible actuation is considered. Considering also stability and transition, in the publication by Min *et al.* [6] blowing/suction at the wall in the form of upstream traveling waves (UPTW) are applied in a turbulent channel flow. Their two- and three-dimensional numerical simulations show that upstream traveling waves in turbulent channel flow reduce the average friction coefficient to a (sub-)laminar level. This is explained by the extra pumping provided by the wall-actuation [7], leading to negative power savings for the proposed strategy. Recently, Bewley [8] has theoretically shown that for any boundary control, the power exerted at the walls is always larger than the power saved by reducing to sub-laminar drag. The net power gain is therefore always negative if the uncontrolled flow is laminar. However, a positive gain can be achieved when the uncontrolled flow becomes turbulent but the controlled flow remains laminar. The conclusion is that the optimal control solution is to relaminarise the flow and thus rendering transition control a viable approach [9]. To this aim, control in the form of downstream traveling waves (DTW) is more promising as previously suggested by the analysis in Refs. [10, 9]. These authors examine the linear stability of channel flow modulated by UPTW and DTW and show that DTW can have stabilising effect on the flow, while UPTW are destabilising.

In this paper we consider the delay of transition to turbulence in two-dimensional boundary layers by means of spanwise modulations of the base flow. The study by Cossu and Brandt [11] showed that Tollmien-Schlichting (TS) waves in the Blasius boundary-layer flow can be stabilised by steady streamwise-elongated perturbations of the streamwise velocity, the so-called streaks, of finite amplitude. In the presence of streaks, *i.e.* with spanwise modulation of the two-dimensional boundary-layer flow, the unstable TS-waves evolve from two-dimensional waves to spanwise modulated waves, referred to as streaky TS-waves [12]. They have similar phase speed as their two-dimensional counterpart and are less unstable. The experiments by Fransson *et al.* [13] confirmed the theoretical predictions and demonstrated that such a stabilising effect can indeed lead to transition delay [14]. In the experiment, streaks are induced in the boundary layer by cylindrical roughness elements placed close to the plate leading edge, with height of about 40% of the boundary layer thickness [15]. A study of the damping characteristics of streaks on two-dimensional TS-waves in boundary layers under pressure gradient was also performed by Bagheri and Hanifi [16] using the parabolised stability equations (PSE); similarly LES was performed by Schlatter *et al.* [17].

In the quest for other possible transition mechanisms in streaky boundary layers, the development of the TS-waves in the presence of streaks and their interaction have been studied in the past. In particular, the nonlinear interaction of finite amplitude TS-waves with streaks received most of the attention [18, 19]. Streaks, however, may experience a fast growth and reach finite amplitude before the TS-waves and therefore the preliminary step taken by Cossu and Brandt

[12, 12] is to consider the streaky boundary layer as a three-dimensional basic flow in which linear three-dimensional waves develop. Tani and Komoda [18] considered the development of viscous waves in a streaky boundary layer. For small TS amplitudes, three-dimensional waves were detected with mode shapes similar to the Blasius TS-waves but with a distinct two-peak (or M-shaped) structure in the rms streamwise perturbation velocity near the wall in the low speed region. Unfortunately, no explicit measure of the growth rates of such waves was provided. Kachanov and Tararykin [20] generated streamwise steady streaks by blowing and suction at the wall and used a vibrating ribbon to generate TS-type waves. They found three-dimensional waves having essentially the same phase speed as the Blasius TS-waves and with essentially the same M-shaped structure mentioned above. Surprisingly, however, these streaky TS-waves did not amplify as they would have done in the absence of the streaks in the same parameter range. Arnal and Juillen [21] detected natural (not forced) TS-type waves riding on the unsteady streaks induced by free-stream turbulence. Grek *et al.* [22] and Boiko *et al.* [23] forced TS-waves with a vibrating ribbon in a boundary layer exposed to free-stream turbulence. Using refined wave detection techniques they found unstable streaky TS-waves, which were, however, less amplified than Blasius TS-waves. These authors attributed the growth rate defect to the stabilising role of the two-dimensional averaged basic flow distortion induced by the streaks; however, they also found that a mere two-dimensional stability analysis of the average velocity profile was unable to predict a correct growth rate. An LES of a spatially developing boundary layer including both TS-waves and free-stream turbulence has been performed by Schlatter *et al.* [24].

More recent work considered also the development of modal instabilities in a streaky boundary layer. The simulations of the interaction between streaks and TS-waves by Liu *et al.* [25] and Schlatter *et al.* [17] show that breakdown occurs through a pattern of  $\Lambda$ -structures, similar to the secondary instability of the TS-waves. However, the streaks set the spanwise length scale which is much smaller than that of the natural secondary instability of TS-waves. Stability analysis performed by Liu *et al.* [26] shows that, indeed, the streak can either enhance or diminish the overall stability of the boundary layer. The stabilising effect is a reduction in the growth rate of the primary two-dimensional TS-wave; the destabilising effect is a secondary instability. The analysis is consistent with Cossu and Brandt [12] who showed that steady streaks reduce the growth rate of primary TS-waves. The simulations in Ref. [25], as well as those by Fasel [27], demonstrate that unsteady streaks, too, reduce the growth rate of the primary TS-waves. However, the role of unsteadiness is found to be more curious when considering the secondary instability due to the interaction of the streaks and TS-waves. Fransson *et al.* [13, 14] studied this interaction for steady streaks and demonstrated that the presence of streaks is always stabilising and suppresses transition. The simulations by Liu *et al.*, however, show that unsteady streaks promote transition. Therefore, the unsteadiness of streaks is significant in promoting breakdown.

The aim of this study is to investigate the details of the stabilisation process observed in the presence of streaks, perform a parameter study on the response to modulations of different scale, examine the robustness of the approach and verify its applicability in the case of bypass transition. It is well known that boundary layers behave as noise amplifiers and the type of disturbances growing are strongly dependent on the characteristics of the ambient noise. At low levels of ambient disturbances, transition to turbulence is caused by the slow, viscous, exponential amplification of Tollmien–Schlichting waves. The most unstable waves are mainly two-dimensional and undergo secondary instabilities when they reach an amplitude of about 1% of the free-stream turbulence [28]. At moderate and high levels of free-stream turbulence, the growth of the TS-wave is bypassed and low-frequency streamwise elongated structures, the streaks, grow in the boundary layer. These break down to turbulence in the form of

isolated spots initiated by inviscid instabilities associated to the shear layers induced by the streaks [29, 30]. The amplification of streaks in the presence of streamwise vorticity is now well understood, the so called lift-up mechanism [31], and is related to the non-normality of the linearised Navier–Stokes equations [32].

In this context, to investigate the robustness of the stabilisation induced by spanwise modulations of the base flow we will perform numerical simulations in a flat-plate zero-pressure-gradient boundary layer where the laminar-turbulent transition is induced by i) two-dimensional TS-waves, ii) oblique three-dimensional waves, iii) two-dimensional and iv) three-dimensional stochastic forcing inside the shear layer and v) free-stream turbulence. In the first case we show how our numerical method is able to reproduce the experimental results and investigate the flow structures induced by the nonlinear interactions of TS-waves and streaks. By using stochastic forcing of given spectrum we examine the performance of the proposed control strategy to different types of incoming disturbances under controlled conditions. Finally, we perform simulation of transition in the presence of free-stream turbulence to validate the previous results in a more realistic noisy environment.

## 2 Simulation approach and disturbance generation

### 2.1 Discretisation and computational box

The presented simulation results are obtained using a spectral method to solve the three-dimensional, time-dependent, incompressible Navier–Stokes equations, namely the code SIMSON [33]. In the streamwise and spanwise directions, Fourier series are used whereas the wall-normal direction is discretised with Chebyshev polynomials. The non-linear terms are evaluated pseudo-spectrally, using the 3/2-rule for dealiasing in the wall-parallel directions. The periodic boundary conditions in streamwise direction are combined with a spatially developing boundary layer by adding a “fringe region” at the end of the domain. In this region, the outflowing fluid is forced via a volume force to the prescribed inflow velocity field, which in this case consists of a Blasius boundary layer profile (zero-pressure gradient) with superimposed optimal streaks (see below). Further description of the fringe method is given in Ref. [34]. The time is advanced with a four-step low-storage Runge–Kutta method for the nonlinear terms and all the forcing contributions, and a second-order Crank–Nicolson scheme for the linear terms and boundary conditions. The latter are chosen of Neumann-type at the upper free-stream boundary.

For all simulations presented in this paper, spatially evolving boundary-layer flow is considered with the inflow located at Reynolds number  $Re_{\delta_0^*} = U_\infty \delta_0^* / \nu = 300$ . This position corresponds to  $Re_x = 32000$ . Here,  $\nu$  is the fluid viscosity,  $U_\infty$  the free-stream velocity and  $\delta_0^*$  the displacement thickness at the inlet. The simulation box has dimensions  $L_x \times L_y \times L_z$  equal to  $2000 \times 60 \times 180$  in the streamwise, wall-normal and spanwise directions, respectively, made non-dimensional based on  $\delta_0^*$ . The physical domain thus extends to about  $Re_x = 590000$  or  $Re_{\delta^*} = 1300$ . Most results are obtained with a resolution  $N_x \times N_y \times N_z$  of  $512 \times 121 \times 128$  grid points. With this resolution the use of large-eddy simulation (LES) is necessary to obtain accurate results in both the transitional and turbulent regions. For this purpose the ADM-RT model is employed [35]. With this model, the effect of the unresolved spatial scales is accounted for by adding to the momentum equations a relaxation term proportional to the high-pass filtered velocity field, *i.e.*  $-\chi H_{N^*} \bar{u}_i$ . Here,  $\chi$  is a model coefficient which is set constant in the present work,  $H_{N^*}$  symbolises the action of the high-order high-pass filter defined in three dimensions, and  $\bar{u}_i$  is the grid-filtered velocity. Further details on the employed filters are given in Ref. [36]. The relaxation term acts as an energy sink and thereby inhibits the build-up of energy near the numerical cutoff. The ADM-RT model was found to be well suited for the spectral simulations

of transitional flows. In particular, the vortical structures during breakdown can be predicted accurately in both the temporal and spatial setting [37], in addition to an accurate prediction of turbulent boundary layers [38]. Note that there is a close connection between the use of the relaxation term as part of governing dynamic equations and an explicit filtering of the velocity field after each time step, see *e.g.* Ref. [39].

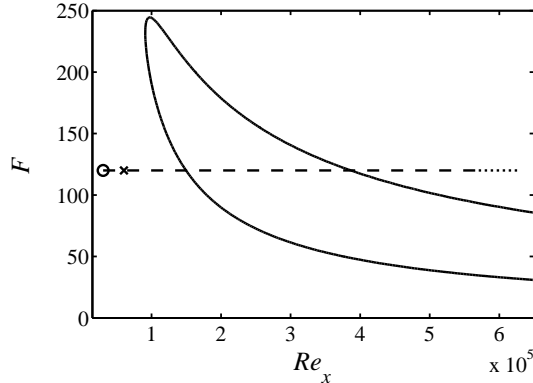


Figure 1: Stability diagram showing the neutral curve for two-dimensional TS-waves; the region enclosed by the solid line corresponds to linearly unstable parameters. The dashed line indicates the computational domain with inlet at  $Re_x = 32000$  ( $\circ$ ), and the cross  $\times$  indicates the streamwise position where the volume forcing is applied. The dotted line is the fringe region downstream of  $Re_x = 590000$ .

## 2.2 TS-wave generation

Two-dimensional (2D) TS-waves used in Section 3 are forced at  $Re_x = 60000$  by a harmonic volume force acting in the wall-normal direction at a non-dimensional frequency  $F = 120$ , corresponding to  $\omega_0 = 10^{-6} F \cdot Re_{\delta_0^*} = 0.036$ , see Figure 1. In this diagram, the region for linearly unstable combinations of the frequency  $F$  and downstream distance measured as  $Re_x$  are enclosed by the solid line. The extent of the numerical domain, shown as the dashed line in Fig. 1 for the given  $F$ , is thus crossing the stability boundary at two  $Re_x$ , commonly referred to as Branch I and II. For most of the cases presented further down the maximum root-mean-square (rms) amplitude of the TS-waves at branch I ( $Re_x \approx 150000$ ) is approximately  $A_{TS} = u_{\text{rms,max}} = 0.76\% U_\infty$ . The validation of the forcing of the TS-waves is presented in Figure 2, which displays the perturbation streamwise and wall-normal velocity profile slightly after branch I in comparison with linear stability theory (LST). Figure 3 shows the growth rate of the wall-normal maximum of the streamwise velocity fluctuation compared to results from solving the (linear) parabolic stability equations (PSE). The TS-waves evolve nonlinearly into a saturated state, therefore also a comparison with lower amplitude forcing is provided in the figure. Good agreement with LST and PSE is obtained by the current LES for both the velocity profile and the growth rate of the TS-waves. The three-dimensional (3D) waves used in Section 4 are forced in a similar way as the 2D waves; in addition to the harmonic time dependence a spanwise dependence of the forcing amplitude is included. This will be further discussed in Sec. 4.

If small-amplitude random noise is also introduced, three-dimensional secondary instability of the two-dimensional waves is triggered, leading to K- or H-type transition shortly after branch II. This nonlinear evolution and breakdown of the TS-waves is also correctly captured by the current LES, as shown in Figure 4 where the classic subharmonic scenario by Herbert [40] is

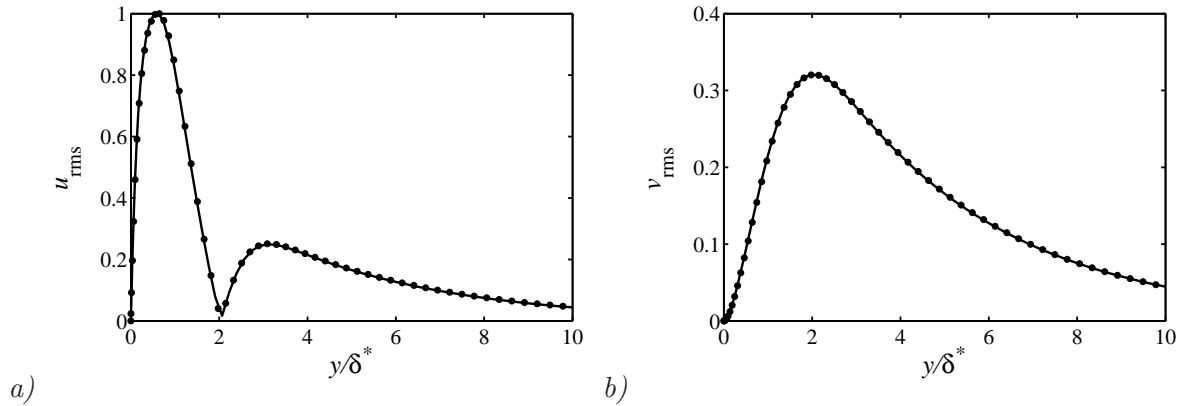


Figure 2: Comparison of the shape of the TS-waves obtained by LES and low-amplitude harmonic forcing with linear stability theory (LST). *a)* streamwise velocity  $u_{\text{rms}}$ , *b)* wall-normal velocity  $v_{\text{rms}}$  at  $Re_x = 216000$  (branch I), — LES, • LST.

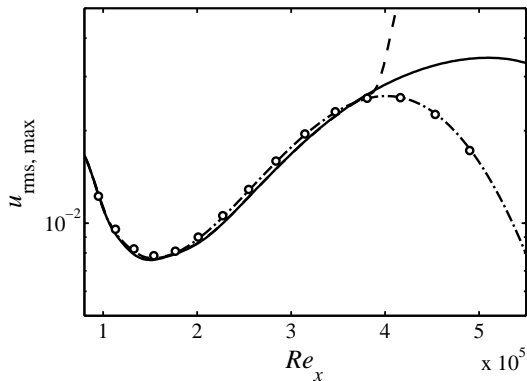


Figure 3: Comparison of streamwise evolution of TS-waves obtained by LES with parabolic stability equations (PSE). Wall-normal maximum of  $u_{\text{rms}}$  for ---- uncontrolled case with random 3D disturbances undergoing laminar-turbulent transition, — 2D nonlinearly-saturated TS-wave, -.- linear low-amplitude TS-wave (rescaled), o linear PSE.

reproduced. In the plot, the evolution of the relevant Fourier components of the perturbation fields is displayed and compared to PSE.

### 2.3 Noise generation

The simulations presented in Section 5 examine the transition behaviour in the presence of stochastic noise introduced into the boundary layer. Similar to the forcing of the 2D and 3D waves, the noise is forced within the computational domain at  $Re_x = 60000$  by a volume force acting in the wall-normal direction close to the wall. Two frequency spectra of the noise are shown in Fig. 5, specifying the noise cases considered as “large-scale” and “small-scale” in the following. For the runs with 3D noise the cut-off spanwise scales are chosen as  $\lambda_{z, \text{max}} = 2.25\delta_{99}$  and  $\lambda_{z, \text{max}} = 0.75\delta_{99}$  for the large and small-scale noise, respectively. The actual amplitude of the noise is determined for each case in such a way that transition to turbulence, *i.e.* the appearance of a turbulent patch, could be observed inside the computational box ( $Re_x < 590000$ ). This will be further discussed in Section 5 and Table 2. A detailed description of the noise-generation method and its practical implementation using temporal Lagrange interpolation is

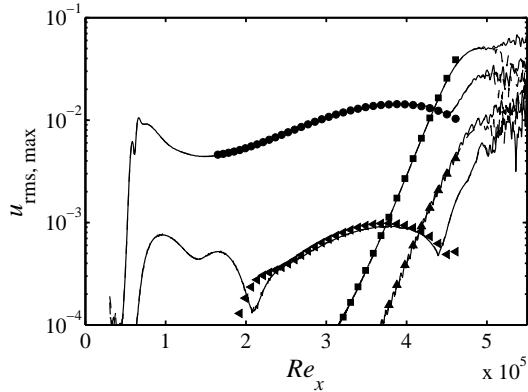


Figure 4: Evolution of various Fourier modes for H-type (subharmonic) transition [40]. — current LES; symbols: PSE.  $\bullet$  mode  $(\omega_0, 0)$ ,  $\blacksquare$   $(\omega_0/2, \beta_{\text{crit}})$ ,  $\blacktriangleleft$   $(2\omega_0, 0)$ ,  $\blacktriangle$   $(3\omega_0/2, \beta_{\text{crit}})$ .

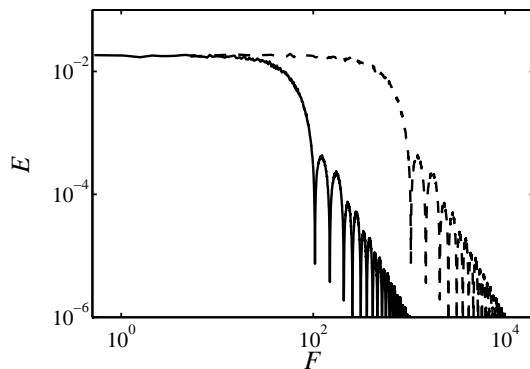


Figure 5: Frequency spectrum of — large-scale and ----small-scale noise. The maximum spanwise scale based on the local boundary-layer thickness  $\delta_{99}$  at the position of forcing ( $Re_x = 60000$ ) for the 3D noise cases is chosen as  $\lambda_{z,\text{max}} = 2.25\delta_{99}$  and  $\lambda_{z,\text{max}} = 0.75\delta_{99}$  for the large and small-scale noise, respectively.

given in Ref. [33]. It is interesting to note that a very similar forcing has been used in direct and large-eddy simulations of spatially evolving turbulent boundary layers as an efficient method to generate initial turbulence, mimicking the effect of a trip wire in windtunnel experiment, see *e.g.* Refs. [41, 38]. In these cases, however, the amplitude of the forcing is chosen larger in order to cause rapid transition to turbulence via the generation of hairpin vortices [42].

## 2.4 Free-stream turbulence generation

A boundary layer developing under the influence of ambient free-stream turbulence (FST) is considered in Section 6. In order to generate approximately homogeneous and isotropic free-stream turbulence at the inflow plane, the approach introduced in Brandt *et al.* [29] is used: A superposition of 800 eigenmodes from the continuous spectrum of the Orr-Sommerfeld/Squire operators is computed to satisfy a given energy spectrum over a range of wave numbers. This superposed disturbance velocity profile is then introduced in the fringe region using the Taylor hypothesis translating spatial streamwise fluctuations into frequency. Further details are given by Brandt *et al.* [29] and Monokrousos *et al.* [2].

## 2.5 Streak generation

The aim of this paper is to quantify the influence of streamwise streaks onto the stability and transition behaviour of a boundary layer. As detailed in the introduction, a number of studies have been performed in experiments using various types of objects placed on the flat wall [13]. In principle, for numerical simulations a similar approach could be chosen, including such obstacles in the numerical domain, *e.g.* using a body-fitted grid or immersed boundary techniques. However, due to the use of a spectral numerical scheme, we have chosen a different approach for the current study: The laminar streaks, characterised by a three-dimensional disturbance field, are introduced at the inlet as optimal disturbances computed from PSE, subsequently evolving nonlinearly inside the domain.

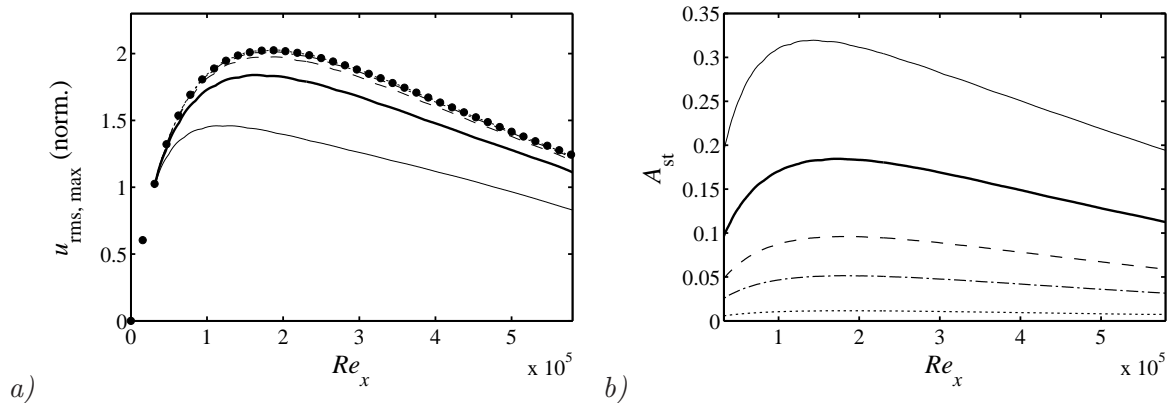


Figure 6: Streak development in the downstream direction. *a)* Streak development for • linear PSE, — streak B, — streak C, ----streak D, -.-streak E, ..... streak G. The streaks are normalised to unit amplitude at the inlet. *b)* Streak amplitude  $A_{\text{st}}$  according to eq. (1).

The complete velocity vector field obtained with the linear code developed by Levin and Henningson [43] is used to force the desired streaky perturbation at the inflow of the computational domain. These streaks are introduced in the fringe region by adding them to the laminar Blasius profile  $U_B$ . The streaks considered are optimally growing perturbations, solution of the linearised boundary-layer equations, and are characterised by the spanwise wavenumber  $\beta_{\text{st}} = 2\pi 10/L_z$  and the streamwise location of their maximum amplitude ( $Re_x \approx 185000$ ). The latter values are chosen to approximately match the streaks in the experiments in Ref. [13]. The different values of the streak amplitudes considered are reported in Table 1. The streak amplitude  $A_{\text{st}}$  is defined as:

$$A_{\text{st}}(x) = \left[ \max_{y,z} (U - U_B) - \min_{y,z} (U - U_B) \right] / 2U_{\infty}. \quad (1)$$

Note that the streak of largest amplitude is susceptible to secondary inviscid instability [44].

The evolution of the streaks in an otherwise undisturbed laminar boundary layer is shown in Figure 6. A validation of the implementation is given in Fig. 6*a)* comparing the streamwise velocity disturbance arising from the developing streaks with the results obtained by PSE: For lower streak amplitudes (*i.e.*  $A_{\text{st}} < 5\%$  at the inlet) very good agreement is observed, indicating that for such amplitudes the effect of nonlinearity on streak development is small. Fig. 6*b)* shows  $A_{\text{st}}$  as a function of downstream distance  $Re_x$ . As the streak is entering the computational domain, it first experiences transient growth, until reaching a maximum amplitude. For all streaks the maximum amplitude is reached at  $Re_x \approx 190000$ , approximately at the same position

Table 1: Amplitudes  $A_{st}$  of the streaks used for the various simulations. Definition of streak amplitude according to eq. (1). Case N corresponds to a case without streaks.

Streak	$A_{st}$ at inlet	$A_{st,max}$	$Re_x$ of maximum amplitude.
A	29%	39%	120000
B	20%	32%	150000
C	10%	19%	170000
D	5%	10%	195000
E	2.6%	5.1%	190000
F	1.7%	3.4%	185000
G	0.6%	1.2%	185000
N	0%	0%	n/a

as Branch I for the TS-waves introduced above. Further downstream, the effect of viscosity will lead to decay of the streak amplitude.

The downstream change of the cross-stream shape of the streak is illustrated in Fig. 7. At the beginning of the domain,  $Re_x = 32000$  as in Fig. 7a), the streak only contains one spanwise wavenumber  $\beta_{st}$ , due to the linearity of the underlying PSE calculation. When comparing to plot b) further downstream, one can note that in the nonlinear simulation the low-speed region, caused by the lift-up of low-speed fluid from the wall, is widening toward the boundary-layer edge for the large amplitude disturbance. At the same time, the region of high-speed fluid near the wall increases its area. This effect, neglected in linear calculations, indicates that the commonly used “shape assumption” for streaks does not hold at such amplitudes. The accurate description of the developed state of a streak necessitates more than one wavenumber  $\beta_{st}$ .

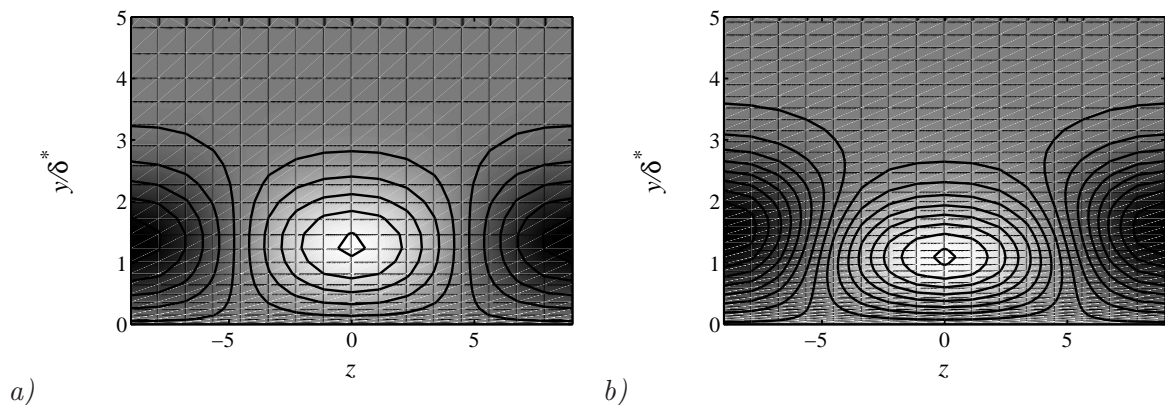


Figure 7: Visualisation of the streak C at a)  $Re_x = 32000$  and b)  $Re_x = 332000$ . Shown is the streamwise disturbance velocity  $u - u_{Blasius}$ , contour spacing  $0.02U_\infty$ , negative disturbance is dark, positive is light. The boundary-layer edge of the Blasius boundary layer is at  $\delta_{99} \approx 2.9\delta^*$ .

### 3 Two-dimensional waves

The results presented in the following are obtained by averaging in time and in the spanwise direction after the simulations have reached a statistically stationary state. The analysis of the spectral contents has been performed by Fourier transforms in time and in the spanwise

direction of a number of full velocity fields saved during one or two cycles of the fundamental period of the primary TS-waves. The corresponding modes are denoted by  $(\omega_0, \beta_{st})$ -pairs in the following. For all the results in this section, the TS-waves are introduced as described in Section 2.2. The details of the streaks are discussed in Section 2.5

### 3.1 Linear TS-waves

The linear evolution of the TS-waves in the streaky boundary layer is considered first. The results for TS-waves with frequency  $F = 120$  are shown in Fig. 8: Starting from the case with TS-waves evolving in a two-dimensional boundary layer (thick line in Fig. 8), streaks of increasing amplitude (streaks B to F, see Table 1) have a stronger quenching effect on the unstable waves; for sufficiently high amplitude of the streaks any growth of the TS-waves is in fact suppressed by the presence of the streaks. This clearly confirms the findings by Cossu and Brandt [11], which have also been reproduced experimentally by Fransson *et al.* [13].

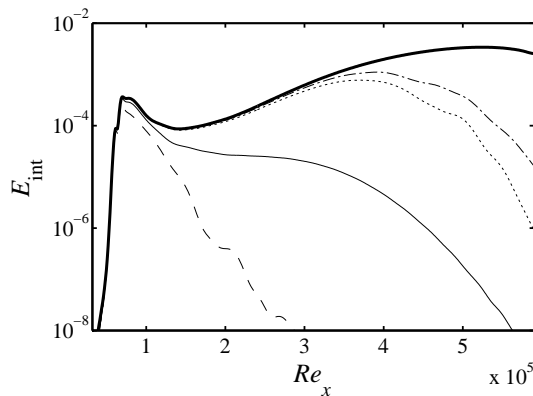


Figure 8: Energy integrated in the wall-normal direction contained in mode  $(\omega_0, 0)$  of the two-dimensional TS waves at  $F = 120$  in the presence of streaks. ----streak B, ——streak C, ..... streak E, -.-streak F, ——no streak (case N). For streak amplitudes see Table 1.

Figure 9a) displays the behaviour of TS-waves of lower frequency in a longer domain. By comparing with the streak amplitude in Fig. 9b) it is evident that the observed stabilisation is related to the local streak amplitude. In the following we will therefore consider only waves with frequency  $F = 120$ , with the assumption that the control effect of streaks of lower amplitude can be related to that of waves of lower frequency. Lower frequencies will be amplified further downstream and will ride on streaks of lower amplitudes; in other words, what is found at lower streak amplitudes can also be observed for stronger streaks, only further downstream and with waves of lower  $F$ . The stabilisation effect appears to be independent of the wave frequency.

The wall-normal disturbance profiles of the streamwise velocity belonging to the streaky TS-waves averaged in the spanwise direction are reported in Figure 10. The typical M-shaped structure [18], *i.e.* featuring two local maxima of the rms values close to the wall, observed in previous numerical and experimental studies, is well captured by the current simulations.

### 3.2 Influence of the spanwise scale of the streak

Simulations of transition featuring TS-waves and streaks under controlled conditions have been performed to investigate the effect of the streak spanwise scale on the stabilisation and possible transition delay. It is observed that if the TS-waves reach sufficiently high amplitudes, *i.e.* of the order of 0.5% of the free-stream velocity, and the streaks are characterised by the spanwise

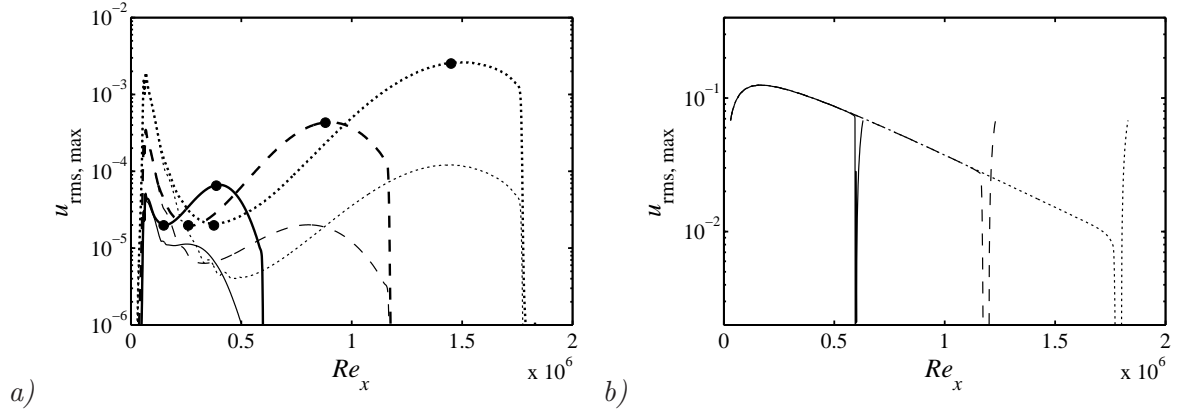


Figure 9: Streak C and 2D TS-waves of different amplitude and frequency. —  $F = 120$ ,  $A_{TS} = 2.575 \cdot 10^{-5}$ , ----  $F = 70$ ,  $A_{TS} = 1.692 \cdot 10^{-4}$ , .....  $F = 50$ ,  $A_{TS} = 1.000 \cdot 10^{-3}$ . a) Mode  $(\omega_0, 0)$ , thick lines are only TS-waves, thin lines controlled with streak C. • position of branch I and II according to LST. b) Streak amplitude  $u_{\text{rms,max}}$ . For this plot the fringe region is not cut away to indicate the end of the computational domain.

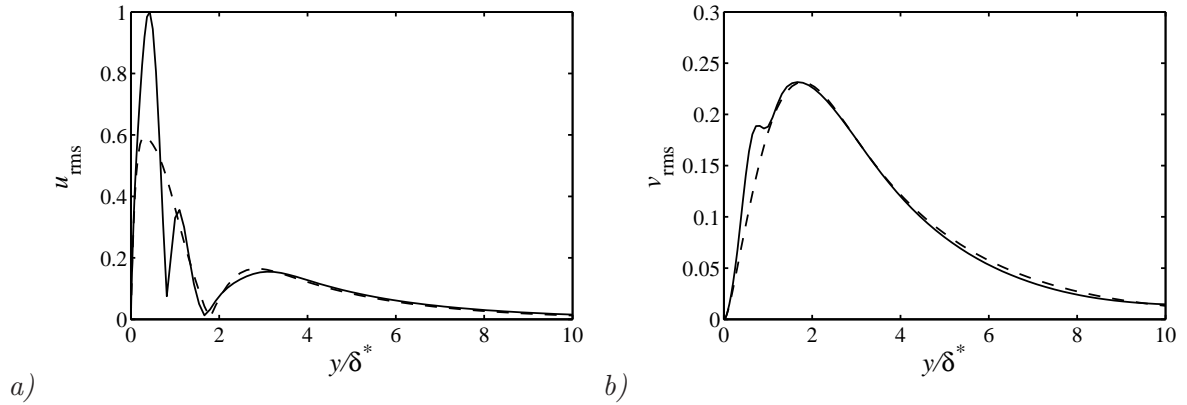


Figure 10: Waveforms of the — streaky TS-waves compared to the corresponding normal TS waves (----) at  $Re_x = 482000$  (streak C, TS-wave with  $F = 120$ , see Fig. 8). The amplitude of the streaky waves is rescaled by 110 to account for the lower growth rate.

scale of the unstable secondary instability modes, turbulent breakdown is indeed promoted by the presence of the steady streaks. If, on the other hand, the streak spacing is chosen too narrow, the coupling between TS-wave and streak is low leading to a reduced damping effect. Therefore, the streak spanwise wavenumber used in the following results is chosen about three times larger than that of the most unstable wavenumber of secondary instability. This scale roughly corresponds to that already used in the experiments by Fransson *et al.* [13].

### 3.3 2D waves with small-amplitude noise

The uncontrolled reference case is given by the two-dimensional forcing at  $F = 120$  exciting two-dimensional TS-waves, and an additional low-amplitude random forcing superimposed onto the harmonic signal. The amplitude of the random forcing is more than one order of magnitude lower than that for the TS-wave. The resulting flow fields are shown in Fig. 11: Initially, the forced TS-waves decay, until they reach branch I (compare Fig. 8), after which an amplification is initiated. In Fig. 11a) and b) this is evidenced by an increasing size of the spanwise

oriented vortices, visualised by isocontours of negative  $\lambda_2$  [45], the second largest eigenvalue of the Hessian of the pressure. Shortly after branch II (corresponding to  $Re_x \approx 400000$ ), the two-dimensional TS-waves show clear signs of a three-dimensional secondary instability in the form of so-called spanwise  $\Lambda$ -vortices. The exact characteristics of this is dependent on the details of the small-amplitude noise forced together with the harmonic TS-waves: Either pure K-type (fundamental), H-type (subharmonic), or de-tuned transition scenarios can be obtained [46, 28, 32]; the two pure scenarios differ in the alignment of the  $\Lambda$ -vortices: K-type transition, Fig. 11*a*), features an aligned formation of  $\Lambda$ -vortices, whereas a staggered pattern is characteristic for pure subharmonic H-type transition. De-tuned scenarios contain a (possibly irregular) mixture of the features of the both the pure K- and H-type scenarios. In Fig. 11*b*) such a flow state is visualised, resembling the pure staggered H-type scenario. The latter scenario is found to be more unstable than K-type transition for most frequencies [28], which is confirmed by the present results showing slightly earlier transition in Fig. 11*b*) than in case *a*). Note that transition in Fig. 11*b*) is induced by superposing small-scale noise of random nature in both time  $t$  and span  $z$  on top of the TS-waves, whereas K-type transition in Fig. 11*a*) is obtained if the noise is random in  $z$  but constant time.

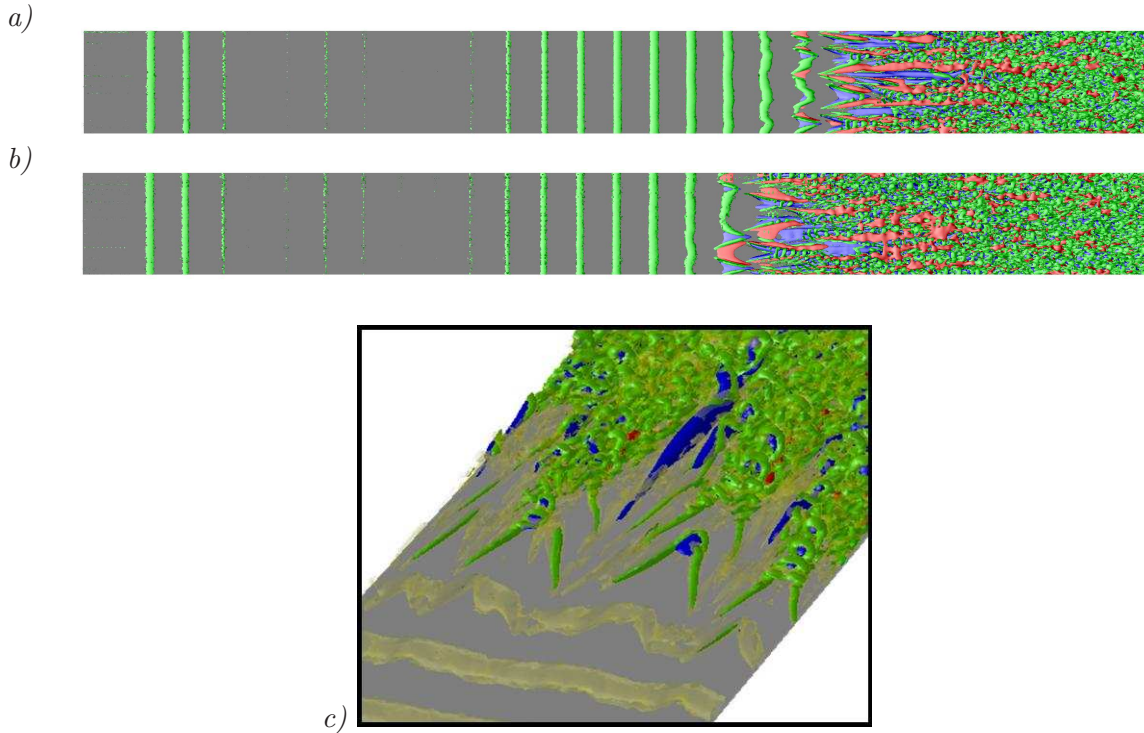


Figure 11: Top view of the three-dimensional flow structures for uncontrolled case N, *a*) steady and *b*) unsteady 3D noise (base-line cases). Green isocontours represent the  $\lambda_2 = -0.00008$  vortex-identification criterion [45], red and blue isocontours are positive and negative disturbance velocity  $u' = \pm 0.07$ , respectively. Flow from left to right. *c*) Three-dimensional impression of the K-type breakdown: Transparent yellow:  $\lambda_2 = -0.00008$ , green  $\lambda_2 = -0.0002$ , blue and red  $u' = \pm 0.1$ .

Next we study cases which feature streaks in addition to the TS-waves. The transition delay obtained in the presence of the steady streaks is displayed in Figure 12. The skin-friction coefficient  $c_f$ , Fig. 12*a*), remains at the laminar value for the two cases with streaks of largest amplitude (streaks C and D), an increase of  $c_f$  by a few percent being only observable where they reach their peak amplitude. The explanation for the observed stabilisation is provided

in Figure 12b) where the shape factor  $H_{12}$  associated to the base flows under consideration is reported. The presence of the streaks progressively reduces the value of  $H_{12}$  in the initial laminar region thus stabilising the flow. Figure 12c) shows the level of streamwise velocity perturbation in the boundary layer, accounting for the presence of the streaks. For large amplitudes of the latter,  $u_{\text{rms,max}}$  is dominated by the steady contribution, so the curves basically display the streamwise streak development. Conversely, in the absence of streaks the perturbation consists mainly of TS-waves and the breakdown can be identified by the sharp rise in the fluctuation level at higher  $Re_x$ . For intermediate values of the streak amplitudes, both the initial amplitude of these spanwise modulation and the breakdown further downstream can be seen.

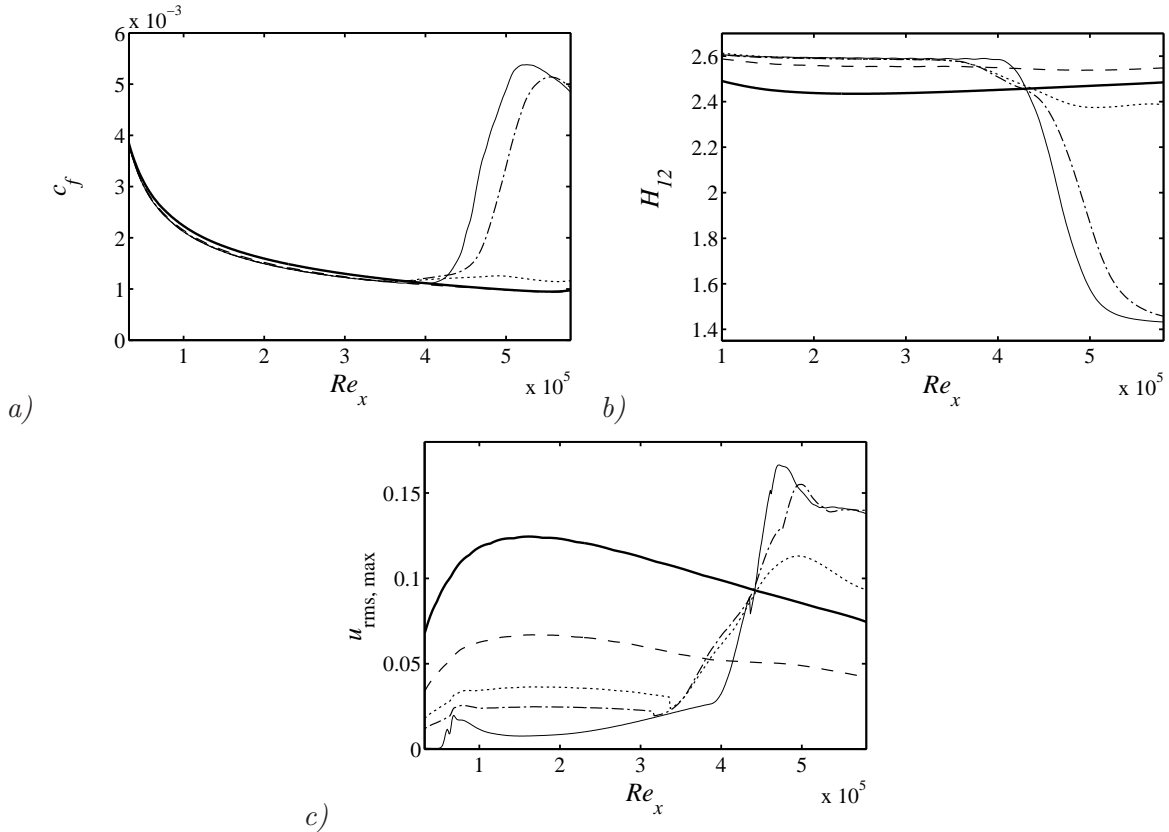


Figure 12: a) Skin friction coefficient  $c_f$ , b) shape factor  $H_{12}$ , and c)  $u_{\text{rms,max}}$  averaged in time and spanwise direction. — Streak C, ----streak D, ..... streak E, -.-streak F, — case N (uncontrolled).

Results of the Fourier analysis are presented in Figure 13 for streaks C, D and E. For the largest streak amplitude, streak C considered in Figure 13a), the fundamental steady streak can be seen as the only dominant mode  $(0, \beta_{\text{st}})$ . Both the two-dimensional and oblique TS-waves are quickly damped, and the first harmonic of the streak  $(0, 2\beta_{\text{st}})$  remains as the second largest mode. For this the mode associated with the TS-wave  $(\omega_0, 0)$  does not experience any significant growth. In this case, the flow is well described by the linear evolution of TS-waves in a spanwise modulated boundary layer as in the analysis by Cossu and Brandt [12].

On the other hand, the simulations with streaks of lower amplitudes, cases D and E,  $A_{\text{st}} = 5\%$  and  $2.6\%$  respectively, (Figs. 13b) and c)) highlight a new physical phenomenon observed at those low streak amplitudes when streaks and TS-waves have similar strength. Thus, more complex nonlinear interactions between both disturbances can take place. Initially, the  $(0, \beta_{\text{st}})$  streaky mode is dominating, reducing the growth of the streaky TS-waves

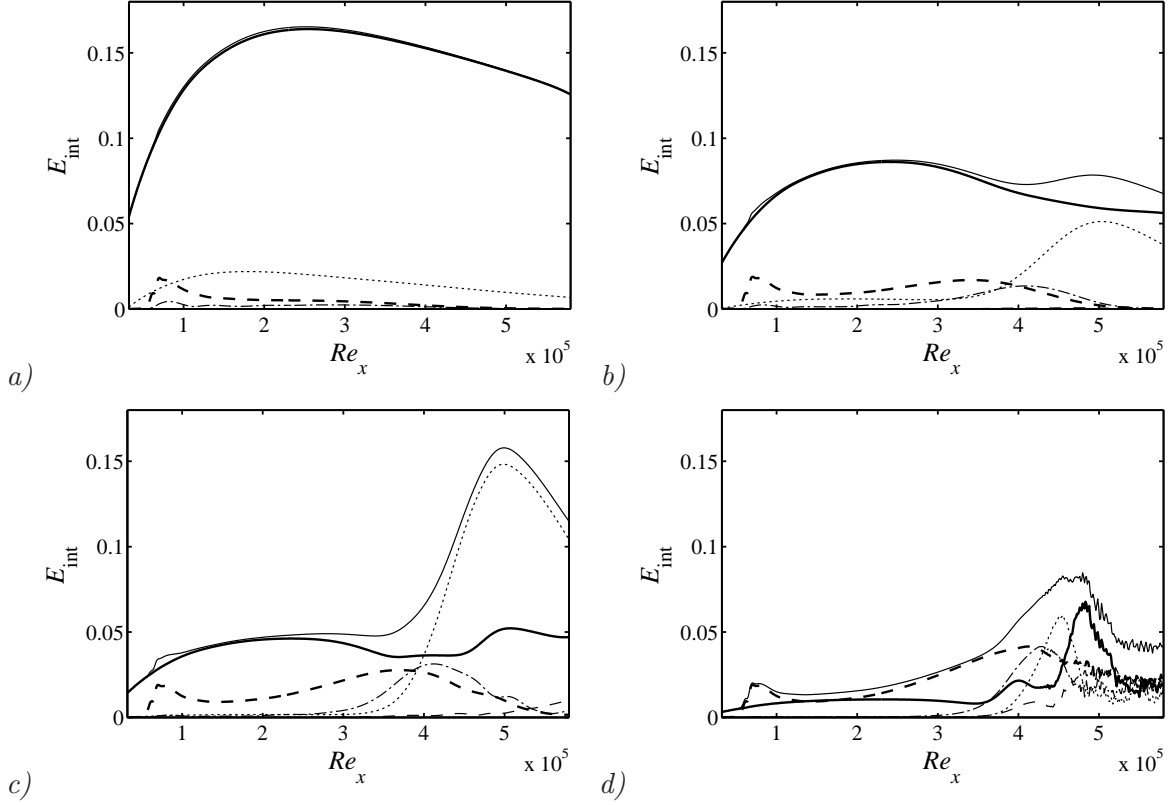


Figure 13: Energy integrated in the wall-normal direction for selected Fourier modes. From *a)* to *d)*: Streaks C, D, E, G, respectively. — Steady streak  $(0, \beta_{st})$ , ---- TS-wave  $(\omega_0, 0)$ , ..... first harmonic of streak  $(0, 2\beta_{st})$ , -- first harmonic of streaky TS-wave  $(\omega_0, \beta_{st})$ , ---- oblique mode  $(\omega_0, \beta_{st}/3)$ , — sum of all displayed modes.

$(\omega_0, 0 \dots 2\beta_{st})$ . Further downstream,  $Re_x > 4 \cdot 10^5$ , however, a significant growth of oblique modes  $(\omega_0, \beta_{st})$  is seen. This induces, by nonlinear interactions, a strong amplification of the steady  $(0, 2\beta_{st})$  mode, *i.e.* a doubling of the initial streaks is observed (see also the visualisation in Figure 16*b*) further down). Towards the end of the domain, growth of the mode  $(\omega_0, \beta_{st}/3)$  can be observed, eventually leading to breakdown further downstream, as partially shown in Figure 16*b*) below). Note that the streak doubling occurs also without the presence of the noise (see below), but in that case it is not followed by turbulent breakdown. The latter is associated to the growth of oblique modes of fundamental frequency and wavenumber close to the natural secondary-instability wavenumber, *i.e.* the mode  $(\omega_0, \beta_{st}/3)$ .

The lowest streak amplitude, Fig. 13*d*) still features some growth of the  $(0, 2\beta_{st})$  mode, however, laminar-turbulent transition and the associated amplification of the energy of the higher modes is occurring shortly downstream of  $Re_x \approx 450000$ . In terms of the modal picture, this case is very similar to the uncontrolled case (not shown).

### 3.4 Flow visualisations

Visualisations of the instantaneous flow field are shown in Figure 14 for seven streak amplitudes, streaks A, C, D, E, F, G and N, and with the same boundary-layer excitation (TS-waves and three-dimensional steady noise, leading to K-type transition). Note that Fig. 14*g*) is the same as in Fig. 11*a*). In these top views of the three-dimensional flow, green isosurfaces indicate vortical structures identified by using the  $\lambda_2$  criterion, whereas isosurfaces in blue and red visualise low-

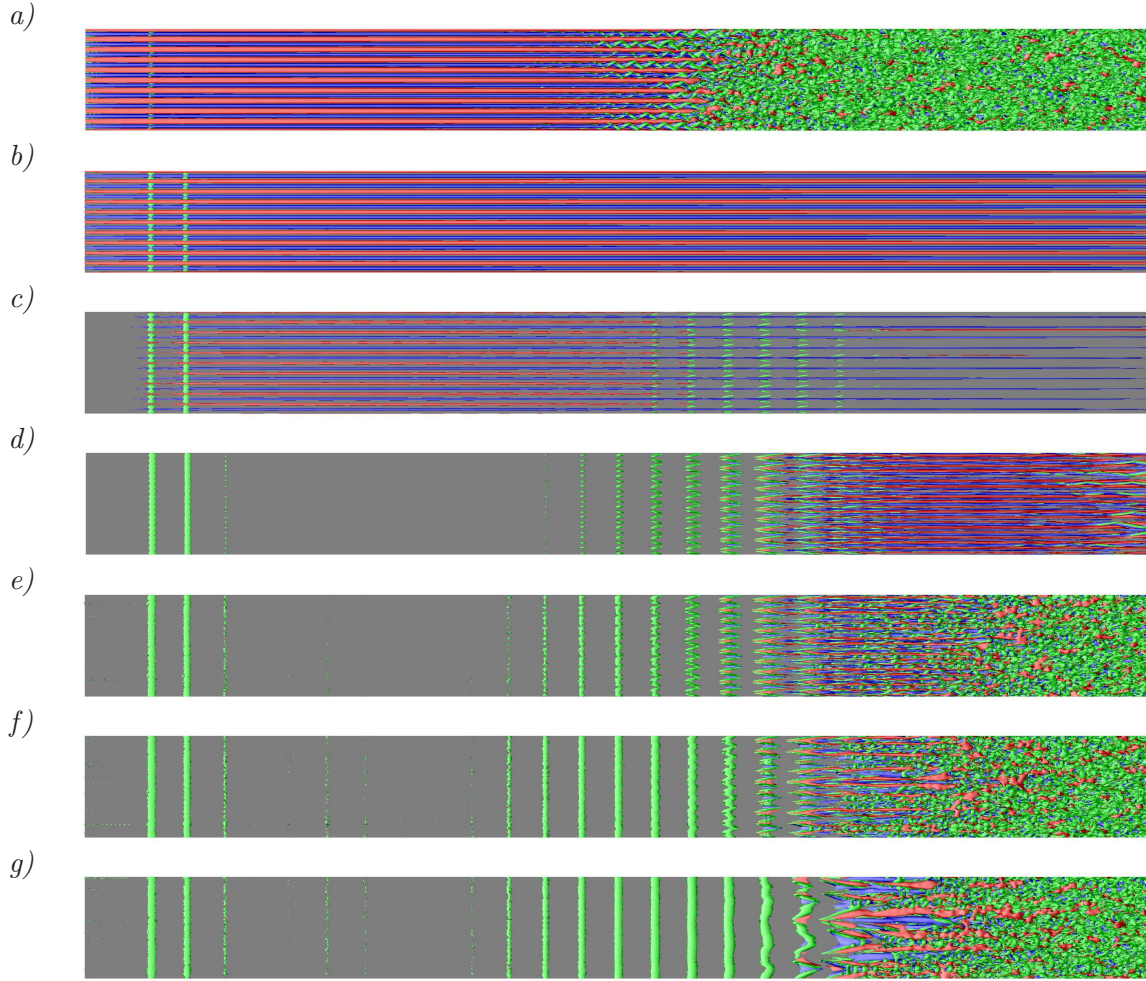


Figure 14: Top view of the three-dimensional flow structures for streaks A, C, D, E, F, G, N (uncontrolled), from *a)* to *g)*. Green isocontours represent the  $\lambda_2 = -0.00008$  vortex-identification criterion, red and blue isocontours are positive and negative disturbance velocity  $u' = \pm 0.07$ , respectively. Flow from left to right.

and high-speed streaks, respectively. In the case of streak A, Fig. 14*a)*, breakdown occurs well within the computational domain. Streak A is indeed unstable to linear perturbations [44]. The relevant vortical structures at the late stage of transition are quasi-streamwise vortices aligned in a staggered pattern and following the spanwise oscillations of the low speed streak. The scenario observed is the same as that arising from the sinuous secondary instability of a steady streak examined by Brandt and Henningson [47]. This scenario has been identified by the latter authors as the most likely to occur in the case of steady streaks of amplitudes  $A_{st}$  larger than approximately 26% of the free-stream velocity. Conversely, streak C is not strong enough to undergo direct secondary instability leading to transition. However, it is strong enough to substantially quench the growth of the TS-waves. In agreement with the experimental findings, a clean spanwise-modulated base flow can therefore be seen in Figure 14*b)*; the slow downstream decay of the streak amplitude is also evident. Further decreasing the streak amplitude, nonlinear development of the TS-waves is observed. For the case in Figure 14*c)* using streak D with steady random noise, this leads to the formation of aligned  $\Lambda$ -structures, associated with the streak doubling discussed above. Considering streak E in Figure 16*d)* amplification of oblique modes is observed at the end of the computational domain, triggering transition of the new streaky

base flow, dominated by the doubled mode  $(0, 2\beta_{st})$ , close to the outflow. For streaks C and D, however, breakdown is not occurring within the computational domain. The streaks of lowest amplitude (streaks F and G), conversely, are not able to reduce the TS-waves enough to prevent transition: turbulent flow can indeed be seen at the end of the computational domain in Figs. 14e) and f). The last plot, Fig. 14g), displays the uncontrolled case. Aligned  $\Lambda$ -structures, typical of the K-type scenario, can clearly be observed. In summary, Figure 14 depicts the various possible transition mechanisms in a boundary layer with streamwise streaks: From the classic K-type scenario (at low streak amplitude) to bypass transition of high-amplitude streaks. In between these limiting cases, stabilisation and transition delay is achieved by means of spanwise modulations of the base flow by means of moderate amplitude streaks.

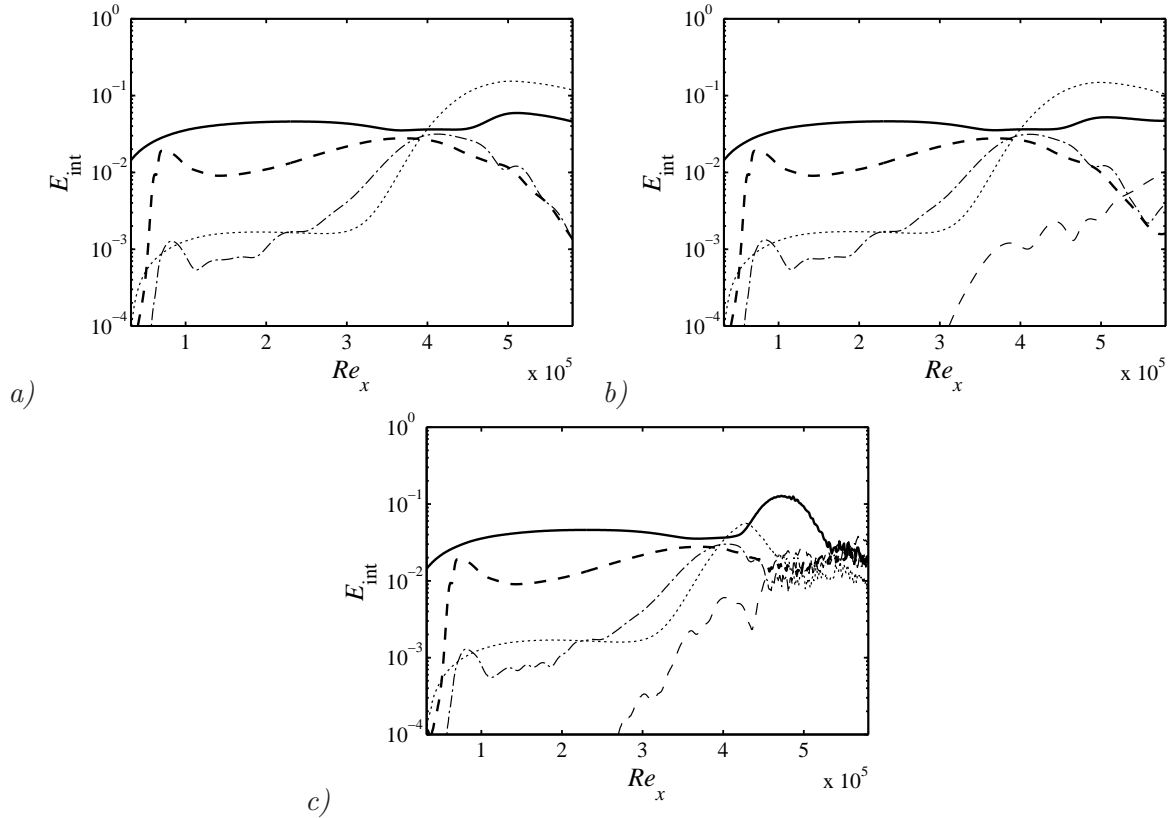


Figure 15: Energy integrated in the wall-normal direction for selected modes for streak E. a) clean TS-wave, b) steady noise, c) unsteady noise. Line caption see Figure 13.

The case of richest nonlinear interaction between streaks and TS-waves of the same order of amplitude, leading to the streak doubling, is further examined in Figures 15 and 16, showing both the modal development and visualisations. Three cases are considered: clean TS-wave without additional small-amplitude noise (not leading to breakdown in the uncontrolled case), steady noise (leading to K-type transition without streaks), and unsteady three-dimensional noise (H-type transition without streaks). Noise obviously needs to be added to trigger laminar-turbulent transition even in the presence of streak E, otherwise all disturbances are decaying at the end of the domain, see Fig. 15a). The streak doubling is however clearly observed in the clean case as well, evidenced by the strong growth of the harmonic of the streak. This particular growth is initially independent of the type of the additional noise, see Figs. 15a)-c). We can therefore conclude that this feature is neither affected nor triggered by the presence of steady or unsteady noise. The streak doubling is associated to the periodic tilting of the streaky TS-

waves into  $\Lambda$  vortices with the spanwise wavenumber of the streaks  $\beta_{st}$ . This spanwise length scale is however much smaller than the one associated to the natural secondary instability of the TS-waves. Similar results have also been obtained in the simulations and stability analysis by Liu *et al.* [25, 26].

In the presence of noise, transition can be observed at the end of the computational domain for both steady and time-dependent small-amplitude forcing:  $\Lambda$  and hairpin vortices can be distinguished in the flow, see Figs. 16*b*) and *c*). In the case of time-dependent noise transition occurs much earlier, however still later than in the uncontrolled case, compare to Fig. 11*c*). The streak doubling is present also in this case even though it is not so evident in the present figure, but can clearly be identified via Fourier transform, Fig. 15*c*). The results confirm that for the parameter settings considered here the subharmonic breakdown is the most rapid one. The computations presented have also been performed with unsteady noise and the results give a picture of the effect of the streaks on the subharmonic transition scenario (and associated delay) similar to the effect on the transition induced by the three-dimensional steady noise.

The figure also shows another important finding: The noise forced upstream obviously survives during the streak doubling process and subsequently determines the transition scenario observed further downstream.

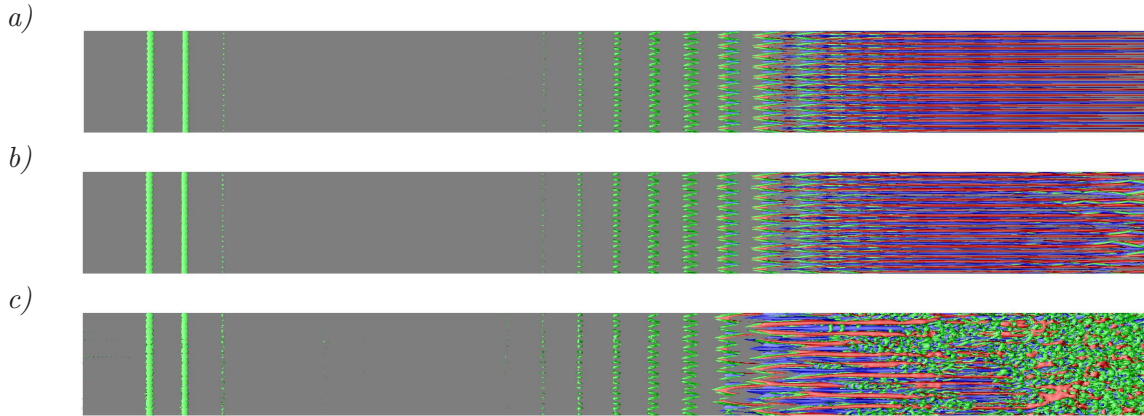


Figure 16: Top view of the three-dimensional flow structures for streak E (same contour levels as in Figure 14). *a*) clean TS-wave, *b*) steady noise, *c*) unsteady noise.

## 4 Three-dimensional waves: Oblique modes

In the previous section, we have observed that two-dimensional perturbations are effectively damped by the presence of streaks, and consequently a transition delay can be achieved for both K- and H-type transition scenarios. This was in full agreement with the initial study by Cossu and Brandt [11] and the experimental confirmation by Ref. [13]. However, before we move to fully three-dimensional and stochastic disturbances, an intermediate step considering the oblique transition scenario is taken. In order to assess the possibility to affect this specific transition scenario by means of streamwise streaks, and to clarify the various influences, a parametric study is carried out where both three-dimensional and two-dimensional forcing is applied in the flow.

To this end, a flow case similar to the baseline simulation presented in Sec. 3, Fig. 11 is considered: TS-waves are forced with fixed amplitude, together with oblique waves of increasing amplitude. Compared to the previous section, the domain width has been chosen  $z_L = 72\delta_0^*$ ,

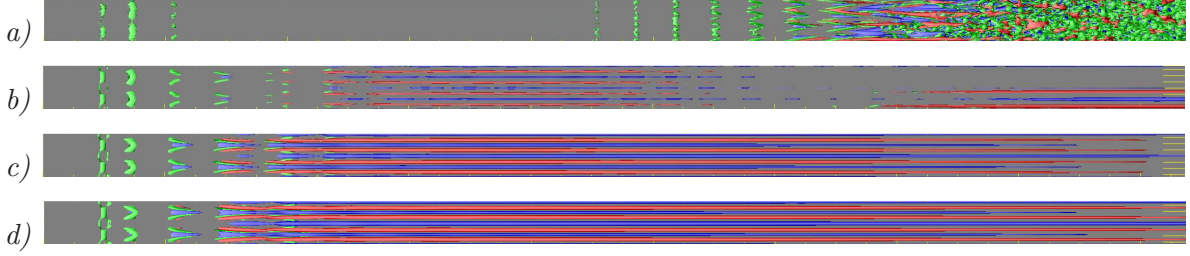


Figure 17: Top view of the three-dimensional flow structures for cases with TS-waves and oblique mode  $(\omega_0, \pm 0.5\beta_{st})$ . a) to d): Increasing amplitudes of the oblique mode  $A_{ow} = 0.005, 0.01, 0.015, 0.02$ . Isolevels as in Fig. 11.

*i.e.* a factor of 2.5 less wide; the spanwise resolution has thus been reduced by a factor of 2 compared to the other runs.

The oblique waves are forced in a similar way as the TS waves through a volume force located at  $Re_x = 60000$ , where the following temporal and spanwise dependency was chosen,

$$f_{ow}(z, t) = A_{ow} \cos(\beta_{ow}z) \sin(\omega_0 t) . \quad (2)$$

Note that  $f_{ow}(z, t)$  is further modified to include a Gaussian streamwise and wall-normal localisation [33]. The resulting oblique mode thus has the Fourier components  $(\omega_0, \pm\beta_{ow})$ . The non-dimensional frequency  $F = 120$ , corresponding to  $\omega_0 = 10^{-6} F \cdot Re_{\delta_0^*} = 0.036$  has been kept for both the TS-waves and for the oblique modes. The spanwise wavenumber of the latter has been chosen to match  $\beta_{ow}/\beta_{st} = 0.5$ , *i.e.* their width is twice the streak spacing. Using the current setup with  $z_L = 72\delta_0^*$ , a total of four spanwise periods of the oblique modes fit into the computational box. The amplitude of the TS-waves is kept the same as in Section 3, while the amplitude of the oblique modes  $A_{ow}$  is gradually increased from 0.005 to 0.02 with a spacing of 0.005.

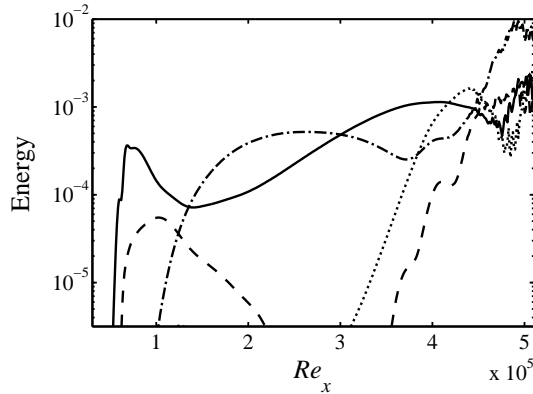


Figure 18: Energy evolution of selected spectral components corresponding to the case with smallest amplitude of the oblique mode in Fig. 17a). — fundamental TS-waves  $(\omega_0, 0)$ ; ---- oblique mode  $(\omega_0, \beta_{ow})$ ; -.- steady modes with wavenumber doubled  $(0, 2\beta_{ow})$ ; ..... first harmonic of the streaky TS-waves  $(2\omega_0, 2\beta_{ow})$ .

In a first step, the interaction of TS-waves and oblique modes is considered. Fig. 17 shows four snapshots corresponding to increasing amplitude of the oblique modes. In Fig. 17a) the dominant primary disturbance is given by the spanwise TS-waves, which is modulated by the spanwise wavenumber of the oblique modes further downstream. Due to the fundamental fre-

frequency  $\omega_0$  of the oblique modes, the classical K-type scenario is recovered. Transition to turbulence is observed towards the end of the computational box.

As the amplitude of the oblique modes is increased, these waves start to interact with each other through a nonlinear mechanism resulting in the growth of a new steady mode with double the spanwise wavenumber [32]. This streak mode is thus associated with the Fourier components  $(0, 2\beta_{ow})$ , and referred to as secondary streaks. This also explains the above choice of  $2\beta_{ow} = \beta_{st}$ , *i.e.* the spacing of the secondary streaks is matching the streak width used for control purposes. In Figs. 17b) to d) the generation of these secondary streaks through a sequence of  $\Lambda$ -vortices is obvious. The effect of these streaks onto the primary TS-waves is now as described in the previous section: The growth of the TS-waves is quenched and transition to turbulence cannot be observed any longer. The final flow is remarkably similar to the visualisation shown in Fig. 14b): The TS-waves have been completely stabilised, and the only remaining boundary-layer disturbance is given by the streamwise streaks.

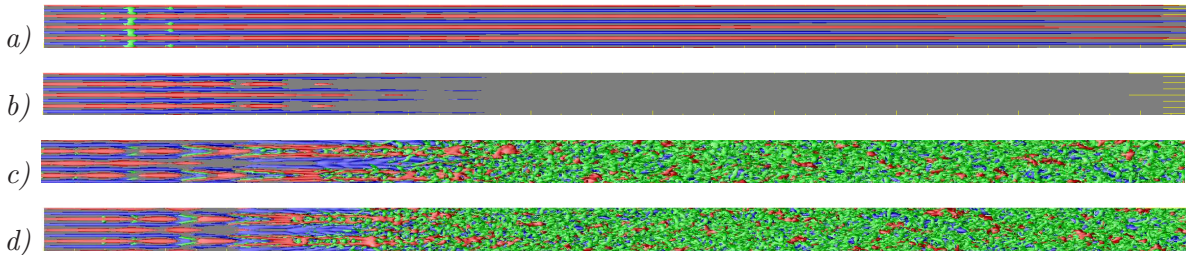


Figure 19: Top view of the three-dimensional flow structures for cases with TS-waves, oblique mode  $(\omega_0, \pm 0.5\beta_{st})$ , and control with streak C. Same amplitudes and isolevels as in Fig. 17.

Fig. 18 shows the streamwise evolution of different Fourier components, allowing us to get additional insight into the departure from the classical K-type transition and on the mechanism which the streak doubling relies on. In the first part of the domain, the forced modes (TS-waves and oblique waves) can be clearly seen as the only dominant modes. The oblique mode itself is strongly damped and its amplitude decreases exponentially. However, as long as its amplitude is relatively large, nonlinear interactions are possible, resulting in the growth of the steady mode  $(0, 2\beta_{ow})$ . The TS-waves, whose branch I and II can be clearly recognised, are therefore affected by the streaks, even though their amplitude is such that a stabilisation cannot be achieved. However, as Cossu and Brandt [11] pointed out, these waves are not bi-dimensional, but they have a spanwise periodicity which agrees with the width of the streaks. In short, new oblique waves, with frequency of the TS-waves and spanwise wavenumber of the streaks, amplify along the domain, as can be observed in Fig. 18. Exactly the same nonlinear interaction leads to new steady modes with wavenumber doubled, *i.e.* the streak doubling observed in the previous section.

In a next series of simulations, in addition to TS-waves and oblique modes, also the streaks are introduced into the domain. These streaks are introduced in the fringe region with a spanwise wavenumber  $\beta_{st}$ , exactly in the same way as in Sec. 3. For the case in Fig. 19a), the streaks are clearly damping the TS-waves, and transition is removed completely. For a slightly higher amplitude of the oblique modes, Fig. 19b), the (intentional) phase shift of the secondary streaks and the control streaks annihilates both streak modes, leaving an essentially undisturbed boundary layer further downstream. However, higher amplitudes of the oblique waves shows a destabilising role of the control streaks: Amplitudes higher than  $A_{ow} = 1\%$  proved to be able to trigger transition in the controlled case. Also, increasing the mode strength is effective on moving progressively the transition point upstream. It should be noted that oblique modes of sufficient amplitude are of course able to trigger transition even in the case without external

Table 2: Parameters of the two- and three-dimensional noise forcing applied at  $Re_x = 60000$ .

Noise type	$u_{\text{rms}}$	$v_{\text{rms}}$	$w_{\text{rms}}$
2D coarse	0.183	0.0332	0.00685
2D fine	0.026	0.00625	0.00455
3D coarse	0.096	0.0074	0.0182
3D fine	0.0655	0.0065	0.0145

streaks, however the chosen amplitudes  $A_{\text{ow}}$  were below that threshold. What the results here show is that strong streaks in a boundary layer are susceptible to instability due to three-dimensional modes, and thus may lower the transition threshold in flow cases that include a significant fraction of 3D disturbances.

## 5 Two- and three-dimensional noise

In this section, the influence onto boundary layer transition of stochastic noise together with streamwise streaks is examined. As opposed to the previous sections 3 and 4, the boundary-layer disturbances are not in the form of a harmonic forcing, but rather stochastic as described in Section 2.3. The noise is introduced inside the computational domain at  $Re_x = 60000$ .

To allow for a general comparison of the influence of noise onto transition, two categories are considered: The dimensionality of the noise (two- and three-dimensional) on the one hand, and the (temporal and spatial) scales of the noise on the other hand. The large-scale noise is centred around modes of spanwise length scale  $L_N = 9$  (only for the 3D cases) and time scale  $t_N = 200$  (corresponding to a non-dimensional frequency  $F = 100$ ), whereas the small-scale noise is characterised by  $L_N = 3$  and  $t_N = 20$ . For the 2D cases, a small amplitude three-dimensional disturbance is added with parameters  $L_{\text{noise}} = 9$  and  $t_{\text{noise}} = 200$  similarly to the TS-wave cases discussed above. The frequency spectrum of the noise is shown in Fig. 5 in Section 2.3.

The amplitude of the noise is determined for each of the four cases in such a way that transition to turbulence, *i.e.* the appearance of a turbulent patch, could be observed inside the computational box ( $Re_x < 590000$ ) for the uncontrolled setup (no streaks). The same noise parameters were then used to investigate the interaction of the noise in the presence of streamwise streaks. The final parameters for each of the cases with noise are listed in Table 2. Depending on the nature of the noise (two- or three-dimensional, scales), different amplitudes had to be chosen: 2D, fine-scale noise proved to be more efficient for reaching transition, requiring  $u_{\text{rms,noise}} \approx 2.6\%$ . On the other hand, 2D large-scale noise was found to be the least effective in provoking transition only with the significantly larger amplitude of 18.3%. The amplitudes required for the three-dimensional forcing lie in between, giving rise to  $u_{\text{rms}}$  amplitudes of around 5 to 10%.

### 5.1 Two-dimensional noise

First, we consider noise that is purely two-dimensional, *i.e.* without spanwise variation. Note that a small-amplitude spanwise-dependent part is added to enable three-dimensional instabilities to grow. As can be seen from Table 2, the amplitude for coarse noise necessary to trigger transition is about  $7\times$  larger than that for small-scale noise. Directly connected to this different amplitudes is the predominant transition scenario observed in the flow. Sample visualisations are shown in Figs. 20a) and c). It becomes clear that 2D small-scale noise in fact leads to the appearance of strong, spanwise uniform waves, similar to TS-waves, compare Figs. 20c) and

11a). These waves oscillate with an approximate frequency of  $F = 200$ , corresponding to the highest growth rate contained in the noise spectrum. The initial amplitude of the TS-waves is sufficient to lead to non-linear breakdown within the computational box. Transition occurs through the classical sequence of  $\Lambda$ -vortices, shear-layer rollup and hairpin vortices. Turbulent spots are seen to originate through the whole domain, i.e. they are not directly generated at the disturbance strip. On the other hand, large-scale 2D noise, Fig. 20a) does not excite any growing instability in the boundary layer for the considered Reynolds numbers. This is due to the fact that two-dimensional waves of low frequency  $F < 80$  are still strongly damped and do not trigger non-modal lift-up mechanism either. Moreover, the disturbance slit is comparably narrow (order  $10\delta_0^*$ ) which does not match the wavenumber  $\alpha$  for a TS wave. Therefore, very intermittent turbulent spots have to be triggered close to the forcing position, which explains the large amplitudes necessary. A spot initiation further downstream (e.g. above  $Re_x \approx 300000$ ) was observed only very seldomly. These turbulent spots then travel downstream while extending in space as seen in the snapshot provided in Fig. 20a).

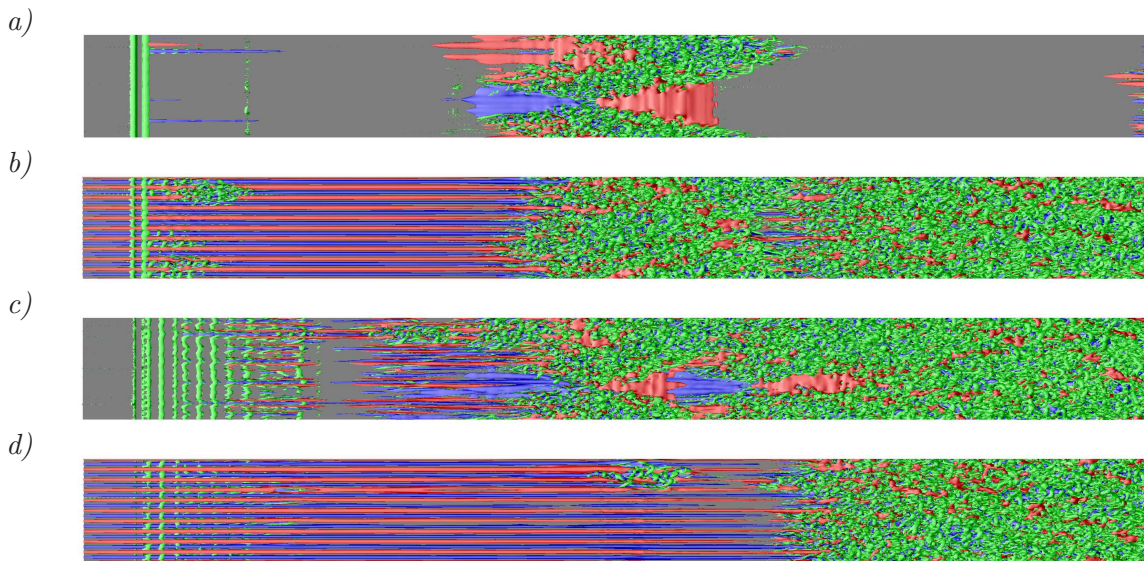


Figure 20: Top view of the three-dimensional flow structures for cases with 2D noise, a), b) large-scale, c), d) small-scale. Same isocontour levels and colours as in Fig. 11. a), c) uncontrolled (no streaks). b), d) controlled with streak C (maximum amplitude  $A_{st} = 19\%$ ).

The efficiency of the imposed streamwise streaks to damp the amplification of disturbances in the boundary layer is naturally strongly dependent on the nature of the growth mechanism and the respective transition scenario. In the previous sections 3 and 4 the damping abilities of streaks have been demonstrated for cases with dominant two-dimensional waves. Consequently, for the case which leads to TS-wave dominated transition (2D small-scale noise), transition delay can indeed be observed when streamwise streaks are added, see the visualisation in Fig. 20d). However, as opposed to cases with clean TS-waves in Section 3 no complete stabilisation of the boundary layer can be achieved; intermittent turbulent spots are appearing further downstream leading to transition. It is important to note that the turbulent spot is no longer triggered by secondary instability of the two-dimensional TS-wave as for the uncontrolled case, but appears as an instability of the strong streaks. This streak instability appears to be similar to the one being discussed further down in conjunction with three-dimensional waves, see e.g. Fig. 24.

Quantitative data for integral parameters of the boundary layer during transition is shown in Figures 21 and 22 for two-dimensional noise forcing. It can be seen that the large-scale forcing

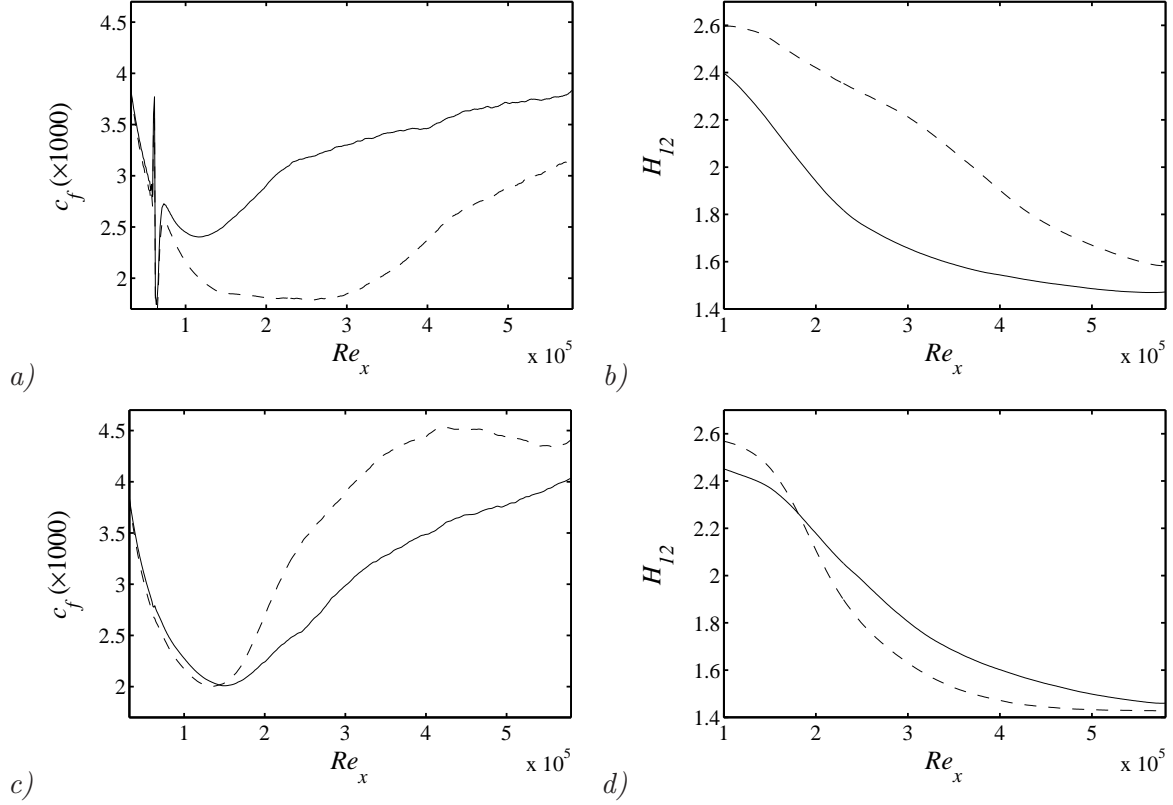


Figure 21: Transition induced by 2D noise. *a)* and *b)*: Large-scale noise, *c)* and *d)*: small-scale noise. Skin friction coefficient  $c_f$  and shape factor  $H_{12}$  averaged in time and spanwise direction. — Streak C, ---- uncontrolled (no streak).

gives rise to very strong peaks at the forcing position  $Re_x = 60000$  visible in for instance in the skin friction  $c_f$ , Fig. 21*a*) and the maximum streamwise velocity fluctuation,  $u_{\text{rms,max}}$ , Fig. 22*a*). For all uncontrolled cases, the shape factor at the inlet is close to the laminar value  $H_{12} \approx 2.59$ , and then slowly decreases as the flow transitions, reaching to values of  $H_{12} \approx 1.4$  typical for turbulent flow at these Reynolds numbers. In a similar way, the skin-friction coefficient  $c_f$  remains initially at the laminar level, until the transition process is taking over. The level of streamwise velocity fluctuations  $u_{\text{rms,max}}$ , Figs. 22*a*) and *b*) experiences clear growth with  $Re_x$ , until a peak at about  $u_{\text{rms,max}} \approx 0.16$  is reached, and the flow settles in a turbulent state.

The introduction of streaks in the presence of large-scale forcing leads to amplified growth of the fluctuations in the boundary layer and thus to transition promotion, see Fig. 21*a*). As mentioned above, the instantaneous views reveal that the large-scale forcing leads directly to the isolated appearance of turbulent spots (Fig. 20*b*). When streaks are present they interact with the large-amplitude noise forcing, generating turbulent patches more frequently and just downstream of the disturbance strip. It was however never observed that the breakdown would occur above  $Re_x \approx 300000$ . This means that if a TS-wave was forced which amplifies further downstream, it is efficiently damped by the streaks. One can conclude that the transition promotion observed in this case is mainly caused by the large amplitude of the noise. However, for the present setup of the numerical experiment, lower amplitude of the large-scale 2D noise would not lead to transition in the uncontrolled case, and consequently no transition delay could be determined from our data. The presence of the streaks also leads to slightly elevated friction levels close to the inlet, and a reduced shape factor  $H_{12} \approx 2.4$  consistent with the mean-flow

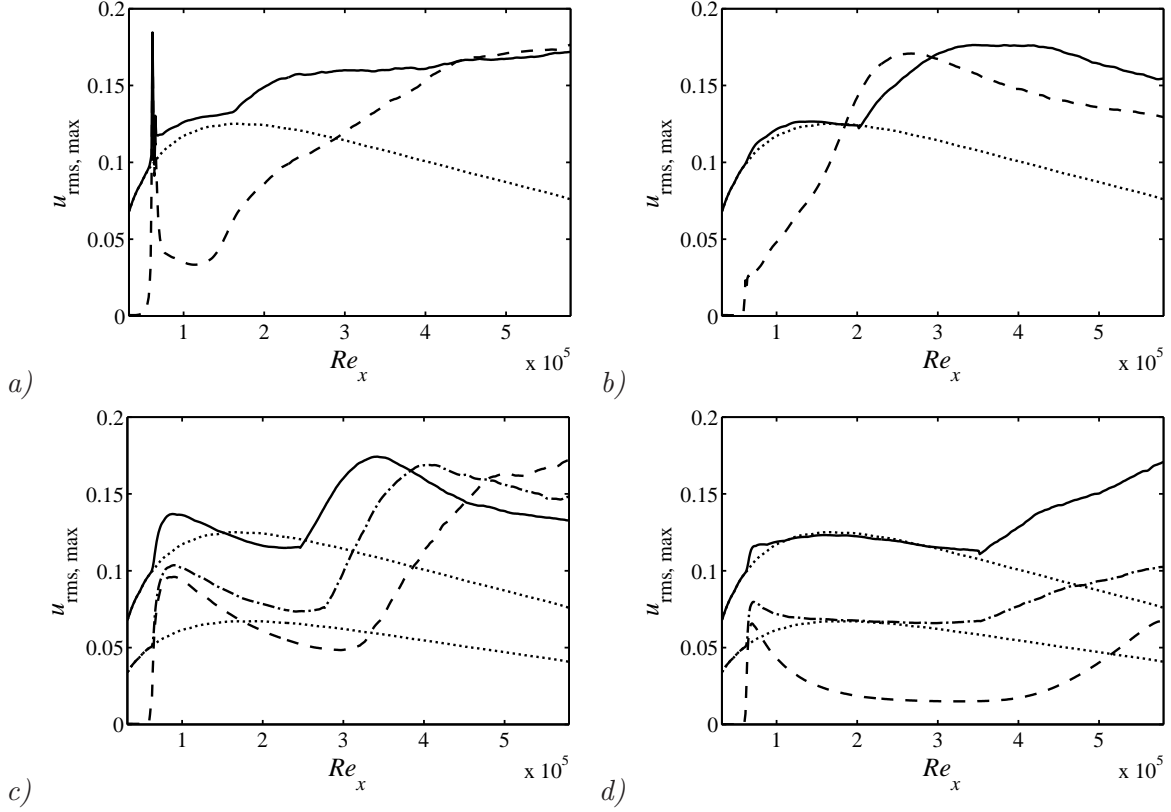


Figure 22: Maximum streamwise fluctuations  $u_{\text{rms,max}}$  as a function of the downstream distance  $Re_x$ . ----only noise (“uncontrolled”), ..... undisturbed streaks (no noise), ——streak C ( $A_{\text{st}} = 19\%$ ), -.-streak D ( $A_{\text{st}} = 10\%$ ). *Top row: 2D noise, bottom row: 3D noise. Left: large-scale noise, right: small-scale noise.*

modification associated with the streaky base flow.

The statistical results pertaining to transition induced by two-dimensional small-scale noise forcing are shown in Figs. 21c) and d) as well as 22b). The introduction of streak C leads to a reduction of skin friction for  $Re_x > 150000$ . The shape factor, although initially lower due to the presence of the streaks, remains at laminar values for a longer time. Similarly, the fluctuation level within the boundary layer is also found to be diminished. The presence of the streak is thus able to delay transition. As discussed above, the visualisation in Figure 20d) clearly shows that the presence of the streaks is in fact damping the waves which were created by the disturbance strip. The intermittent appearance of turbulent spots is occurring over the whole domain, mainly due to an instability of the streak.

## 5.2 Three-dimensional noise

Completely three-dimensional noise is considered next. In this case, no dominant spanwise waves are forced. As before, two spectral ranges in both spanwise and temporal scale of the noise are considered, i.e. low frequency and high frequency. The rms amplitudes used are in the range 5-10% (see Table 2), i.e. somewhat larger than the small-scale 2D noise. Snapshots of the velocity fields for both controlled and uncontrolled cases are shown in Fig. 23.

For the cases with 3D noise, the dominant instability mechanism is non-modal growth based on the lift-up mechanism, generating streamwise streaks. Again, a dependence of the arising flow structures on the scales of the disturbances is observed: Fine scales tend to decay quickly,

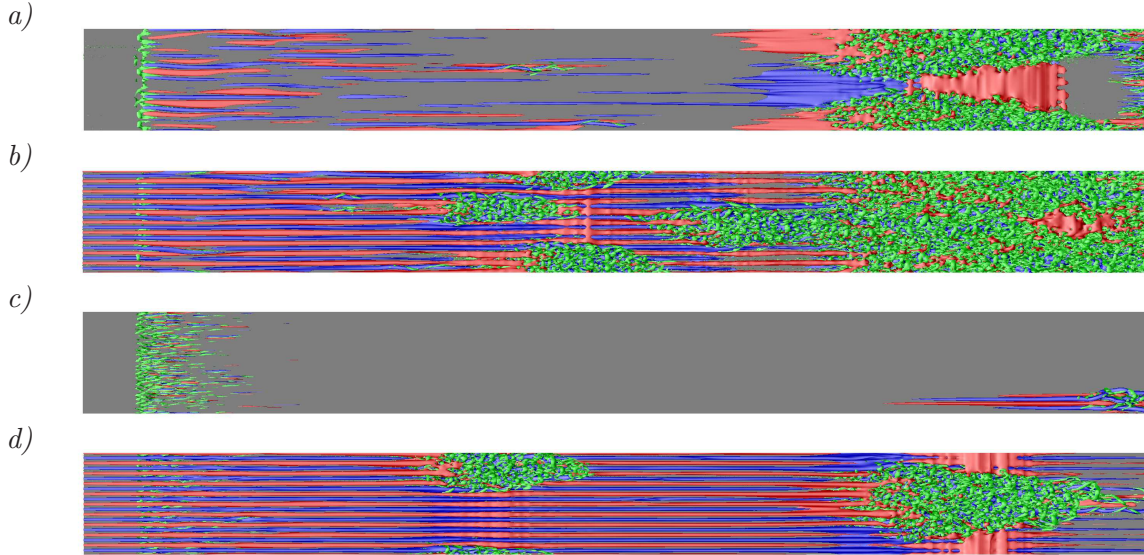


Figure 23: Top view of the three-dimensional flow structures for cases with 3D noise, *a)*, *b)* large-scale, *c)*, *d)* small-scale. Same isocontour levels and colours as in Fig. 11. *a)*, *c)* uncontrolled (no streaks). *b)*, *d)* controlled with streak C (maximum amplitude  $A_{st} = 19\%$ ).

whereas larger scales lead to a flow with significant streamwise streaks, which later become unstable developing a growing wave packet [48] and finally break down into triangle-shaped turbulent spots. This behaviour is clearly demonstrated in Fig. 23*a)*. Note that the arrow-head shaped turbulent spot is wrapped around the spanwise periodic boundaries. A blow-up of the two instabilities located in the middle of the domain is given in Fig. 24. These flow structures appearing in these cases are clearly similar to observations in bypass transition induced by ambient free-stream turbulence [29] and to an impulse response on a steady streak [48]. As a comparison, Figs. 24*c)* and *d)* are taken from Schlatter *et al.*, Figs. 8*c)* and 12*d)*.

For the fine-scale noise, the observed flow behaviour is in principle similar, however due to the faster decay of the boundary-layer disturbances strong streaks are formed less regularly and tend to reach sufficient amplitude further downstream. For the present case, the turbulent spots seem to arise at positions where the noise disturbance has been able to generate a packet of localised streaks, and the spots stem from an instability of the streak itself [47].

Quantitative data of  $c_f$ ,  $H_{12}$  and  $u_{rms,max}$  are shown in Figs. 22*c)* and *d)*, and Fig. 25. As for the 2D cases, the uncontrolled simulations feature an essentially laminar behaviour, with a gradual change towards turbulent values due to the intermittent generation of turbulent spots. Note that for the large-scale noise both  $c_f$  and the shape factor show a small departure from the laminar values due to the appearance of streaks with growing amplitude.

Introducing large-amplitude streaks at the inlet, *i.e.* a spanwise periodic base flow, does not lead to any transition delay, independent of the scales of the noise. To the contrary, turbulent spots can be observed more frequently and they appear further upstream, see Fig. 23*b)* and *d)*. As for the uncontrolled case, the transition scenario is a secondary instability of the streak, characterised by a growing wave packet riding on the streak [48]. Owing to the larger amplitude of the streaks in the case with superimposed steady streaks at the inlet, the streak breakdown occurs further upstream. In the bottom row of Fig. 22 these cases with 3D noise are shown; the breakdown location is clearly moving upstream as soon as streaks are introduced. Similarly, the integral parameters shown in Fig. 25 exhibit the same behaviour. It is interesting to note that an increase of the streak amplitude directly leads to an upstream movement of the transition

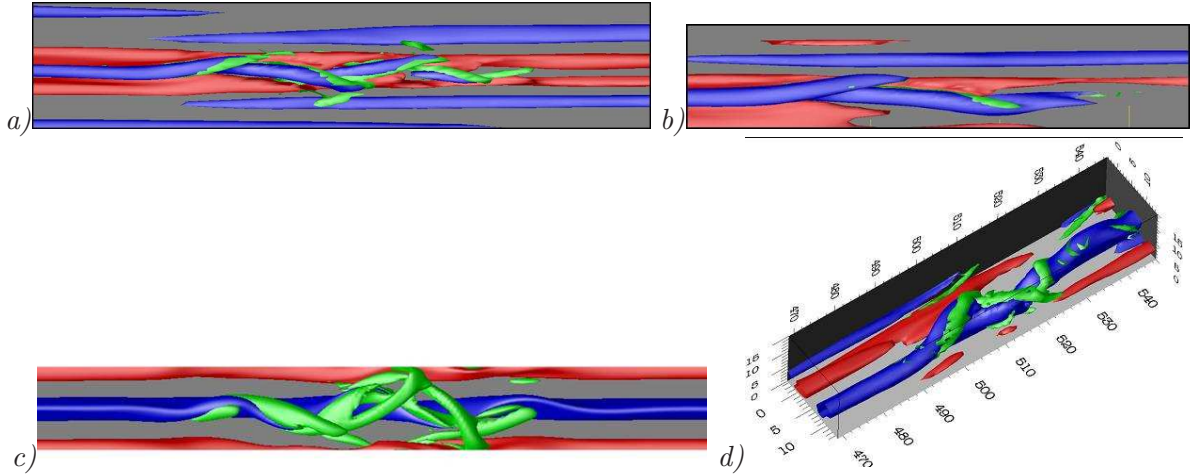


Figure 24: *a)* and *b)* Blow-up of two regions in the middle of Fig. 23 identifying the flow structures just prior to breakdown into a turbulent spot. *c)* Flow structures for a nonlinear impulse response on a steady streak, and *d)* incipient turbulent spot in bypass transition [29]. The latter two pictures are taken from Figs. 8c) and 12d) in Ref. [48].

location, which clearly supports the finding that a streak instability is the dominant cause of breakdown.

The visualisations provided in Figs. 23b) and c) do not show major qualitative differences compared to the uncontrolled cases: the spot precursors are similar to the blow-ups presented earlier, resembling a sinuous streak instability. Notice however that in the presence of strong streaks – irrespective of whether they are actively introduced in the flow or naturally arise due to *e.g.* free-stream turbulence, turbulent spots do not feature a clear triangular shape as they would in a calm boundary layer [49].

It can be concluded that the passive control mechanism based on a spanwise modulated base flow (streamwise streaks) and the subsequent damping of the growth of TS-waves is efficient for transition scenarios based on the modal growth of essentially two-dimensional disturbances, as demonstrated in Section 3. On the other hand, if transition is induced by non-modal growth mechanisms related to bypass transition, the addition of a strong base-flow modulation leads to premature transition, as the general disturbance level in the boundary layer is enhanced.

## 6 Free-stream turbulence

In boundary layers with ambient free-stream turbulence (FST) intensities  $Tu$  of about 1% or less, laminar-turbulent transition is dominated by the classical scenario, *i.e.* exponential growth of Tollmien-Schlichting (TS) waves [32]. As the TS-waves reach amplitudes of around 1% of the free-stream velocity  $U_\infty$ , they experience resonant three-dimensional amplification and break down into a turbulent spot by formation of  $\Lambda$  and hairpin vortices. However, in the presence of higher levels of FST, transition occurs more rapidly, bypassing the classical scenario. The new scenario, denoted bypass transition, is characterised by the formation of streamwise streaks of alternating high and low streamwise velocity, whose amplitude grows downstream and can reach values on the order of  $0.1U_\infty$  prior to breakdown [23, 29].

In this section, two different aspects of a boundary layer under free-stream turbulence are considered. In a first part, Sec. 6.1, it is investigated whether the streamwise streaks induced by free-stream turbulence are causing a change in the growth rates of TS-wave inside a boundary

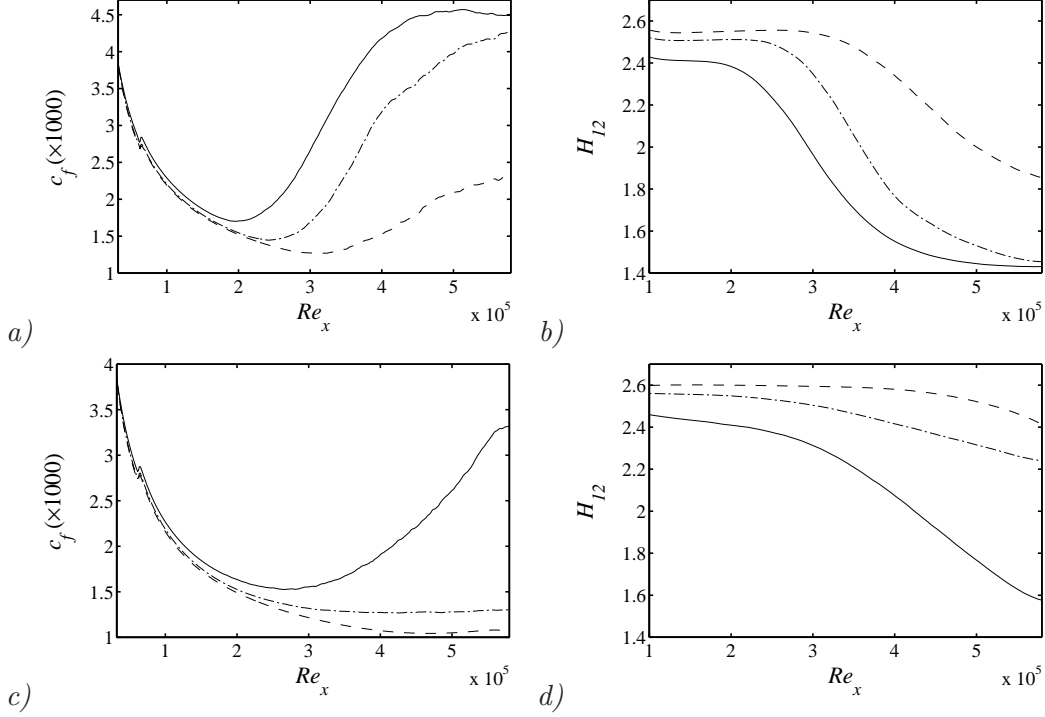


Figure 25: Transition induced by 3D noise. *a)* and *b)*: Large-scale noise, *c)* and *d)*: small-scale noise. Skin friction coefficient  $c_f$  and shape factor  $H_{12}$  averaged in time and spanwise direction. — Streak C, ---streak D, - - - uncontrolled (no streak).

layer. The second aspect, discussed in Sec. 6.2, is whether an external forcing of boundary-layer streaks might be used to delay transition induced by free-stream disturbances (*i.e.* bypass transition).

## 6.1 Interaction of TS-waves and free-stream turbulence

In the following, the effect of FST on the behaviour of TS-waves is studied, including modified growth rates, change in transition location, and transitional flow structures in comparison with both pure bypass and classical (*e.g.* K-type) transition. As usual, the TS-waves are introduced as harmonic volume forcing at  $Re_x \approx 60000$  as described in Sec. 2.2; the free-stream turbulence is forced in the fringe region according to Section 2.4. The two control parameters at hand are the amplitude of the TS-waves  $A_{TS}$  and the free-stream turbulence intensity  $Tu$ . For the TS-waves, two different amplitudes are considered:  $A_{TS} = u_{\text{rms,max}} = 0.76\%$  and  $A_{TS} = 1.52\%$  (measured at branch I,  $Re_x = 150000$ ,  $F = 120$ ). Small-amplitude steady, spanwise random noise is also added to trigger K-type transition after branch II ( $Re_x = 387000$ ) in the case  $Tu = 0$ , as discussed for the baseline case, Fig. 11 in Sec. 3. The turbulence intensity  $Tu$  has been varied from 0 to  $4.7\%U_\infty$ , measured at the inlet,  $Re_x = 30000$ .

In Fig. 26, instantaneous flow visualisations for a fixed TS-wave amplitude  $A_{TS} = 0.76\%$  and different values of  $Tu$  are presented. For the case with  $Tu = 0\%$ , Fig. 26*d)* the baseline simulation is recovered, Fig. 11*a)*. On the other hand, the case with  $Tu = 4.7\%$ , Fig. 26*a)*, is clearly dominated by the free-stream turbulence: The flow field shows the appearance of streaks and the localised breakdown to turbulence on isolated streaks [29, 24]. The intermediate cases are however most interesting: For  $Tu = 2\%$ , Fig. 26*c)*, the TS-waves can still be seen as a distorted signature after branch I. The overall transition location does not appear to change

from these instantaneous snapshots. The breakdown scenario for that case appears to be a mixture between the roll-up of  $\Lambda$  vortices (due to TS-waves) and intermittent turbulent spots due to the presence of the streaks linked to the external turbulent flow. This condition can somehow be seen as the one where the switch from one scenario to another happens. It is interesting to note how these simulations show a similar behaviour as those where the effect of oblique waves was investigated in the uncontrolled case. This is not unexpected since both perturbations, oblique waves and free-stream turbulence, mainly result on the development of streaks. However while the former are steady, the latter change with time and appear randomly throughout the box.

Increasing the turbulence level slightly to  $Tu = 3\%$ , see Fig. 26*b*), the signatures of the TS-waves cannot be distinguished any longer. In addition, the amplitude of the streaks inside the boundary layer, generated by the interaction with the external turbulence, has clearly increased. What is most important, however, is that the transition location appears to have moved downstream towards the end of the computational box. This means that the TS-waves have been effectively stabilised by the action of the free-stream turbulence when  $Tu$  is low. The mechanisms for boundary layer transition, wavepackets of high-frequency perturbations on individual streaks, are still those observed for breakdown induced by three-dimensional noise.

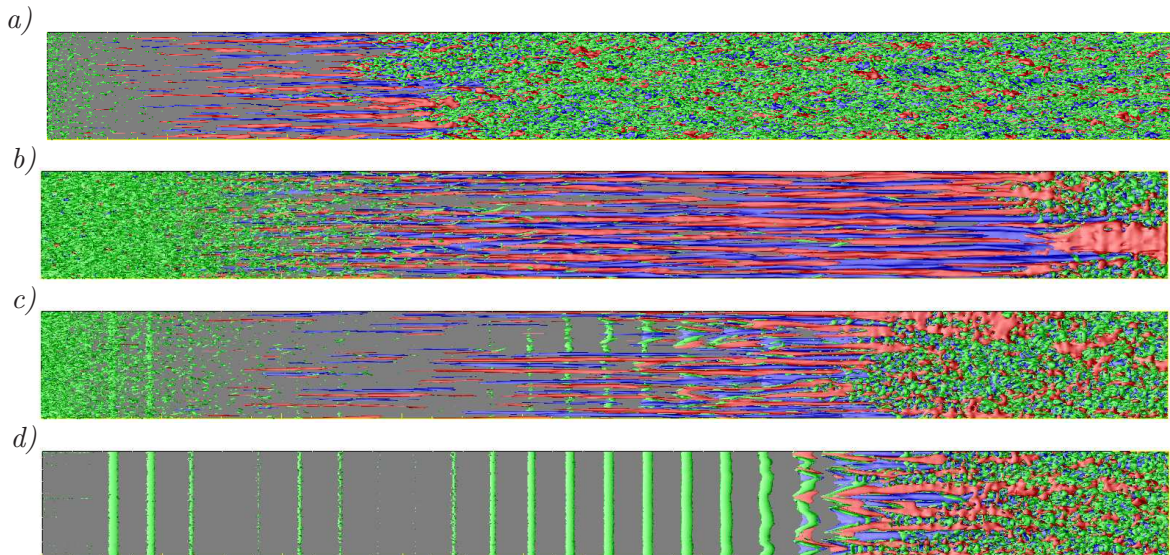


Figure 26: Top view of the three-dimensional flow structures for  $A_{TS} = 0.76\%$ . *a)* to *d)* FST turbulence intensity  $Tu = 4.7\%, 3.0\%, 2.0\%, 0\%$ . Green isocontours represent the  $\lambda_2 = -0.0008$  vortex-identification criterion, red and blue isocontours are positive and negative streamwise disturbance velocity  $u' = \pm 0.07$ , respectively (in *a*) slightly higher contour levels than other cases). Flow from left to right.

Quantitative data for these flow cases are shown in Fig. 27. The initial reduction of the shape factor  $H_{12}$  in the laminar region with increasing  $Tu$  clearly shows the stabilising effect of the streaks [11]. For instance, for  $Tu = 2\%$  the shape factor is reduced to approximately 2.5 at  $Re_x = 3 \cdot 10^5$ . The later dramatic reduction towards turbulent values  $H_{12} \approx 1.5$  is due to transition. The initial reduction in shape factor, however, is caused by the non-modal growth of streaks in the boundary layer, as evidenced in Fig. 27*b*) by the increase of  $u_{rms,max}$ . In agreement with studies on bypass transition [29], breakdown to turbulence occurs when the mean fluctuation level inside the boundary layer reaches values on the order of 10-15%. On the other hand, comparing solid lines ( $A_{TS} = 0.76\%$ ) with dashed ones ( $A_{TS} = 0\%$ ) in Fig. 27, it can be inferred that the initial streak growth is mainly unaffected by the presence of TS-waves.

It is only for higher  $Re_x$  that a difference between solid and dashed lines can be observed.

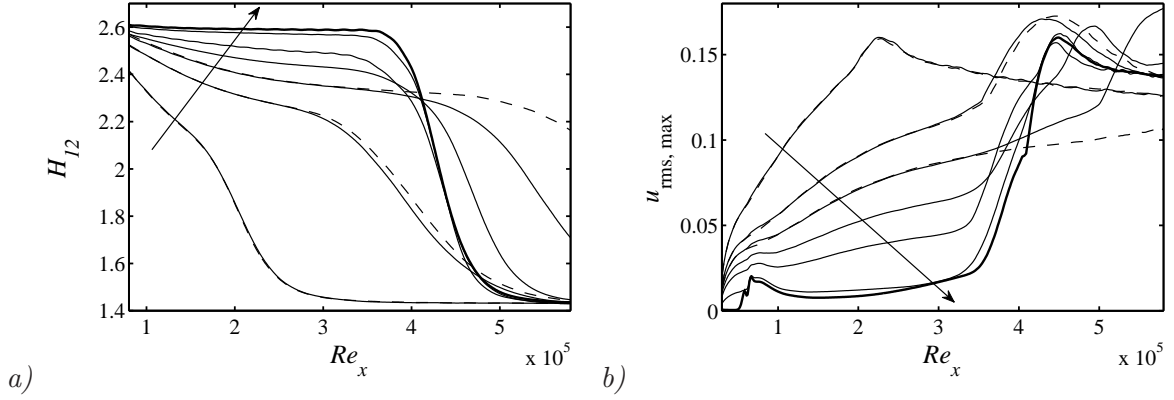


Figure 27: a) and b): Evolution of the shape factor  $H_{12}$  and the wall-normal maximum of the streamwise fluctuation  $u_{rms}$ , respectively, for cases with FST and TS-waves,  $A_{TS} = 0.76\%$ . Arrows indicate decreasing turbulence intensity,  $Tu = 4.7\%$ ,  $3.5\%$ ,  $3\%$ ,  $2.5\%$ ,  $2\%$ ,  $1\%$ , — only TS-wave forcing ( $Tu = 0\%$ ), ---- only FST ( $A_{TS} = 0\%$ ).

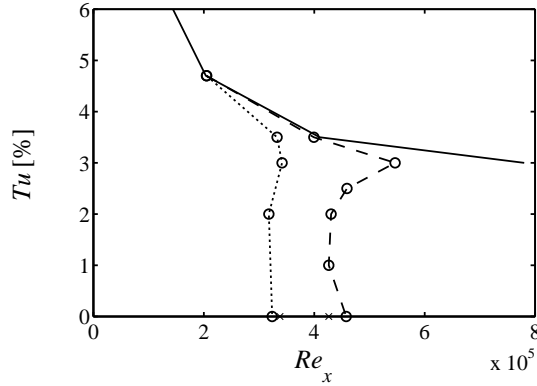


Figure 28: Variation of the downstream position of the transition point  $\gamma = 0.5$  as a function of the turbulence intensity  $Tu$ , — no TS-waves ( $A_{TS} = 0\%$ , pure bypass transition), ----  $A_{TS} = 0.76\%$ , .....  $A_{TS} = 1.52\%$ . The region to the right of each line corresponds to turbulent flow; the region to the left indicates laminar flow.

In Fig. 28 the variation of the transition location (defined as the point where the intermittency reaches  $\gamma = 0.5$ ) is shown for different turbulence intensities  $Tu$  and TS amplitudes  $A_{TS}$ . The solid line shows the case where no TS-waves are introduced and it thus represents pure bypass transition. No transition is observed within the simulation domain for  $Tu$  lower than  $3\%$ . However, when TS-waves are introduced into the flow with the given amplitudes, the exponential amplification of the TS-waves allows secondary instabilities close to branch II to take place, leading to transition.

There are a few important conclusions that can be drawn from this figure: First, it is clear that for fixed  $Tu$  the presence of TS-waves always leads to transition promotion. This effect is weak for higher  $Tu$  and the different curves tend to fall on top of each other. This region is, in fact, dominated by the bypass-transition scenario rather than classical transition, and the TS-waves, still destabilising, play just a secondary role in the breakdown. For  $Tu$  lower than  $3\%$ , on the other hand, transition is increasingly dominated by the modal growth of TS-waves

and the corresponding breakdown. Here, the stabilising effect of the streaks onto the TS-waves become clear: The streaks formed by lower levels of FST actually damp the growth of the TS and lead to transition delay compared to the case without FST. This is particularly clear for  $A_{\text{TS}} = 0.76\%$  and  $Tu = 3\%$ . Under these conditions, visualised in Fig. 26b) the free-stream turbulence is able to produce streaks strong enough to damp the TS-waves, but sufficiently weak to not trigger premature bypass transition: A transition delay of about 20% is achieved. This result agrees with the findings of Ref. [23] who performed experiments with both FST and TS-waves and found that the TS growth rate within a streaky flow is reduced, as long as the TS-waves and FST are at modest amplitudes. On the other hand, it is also clear from Fig. 28 that TS-waves never have a stabilising effect on FST induced bypass transition.

## 6.2 Control of bypass transition

In this section, it is examined whether introducing streamwise streaks into a boundary layer might be useful as a passive control method to delay transition due to free-stream turbulence. As in the previous section, the free-stream turbulence and the streaks are added in the fringe region (see Sections 2.4 and 2.5). Two levels of ambient turbulence intensity are considered:  $Tu = 3\%$  and  $4.7\%$ . As can be seen in Fig. 27, the former FST level leads to transition towards the end of the simulation domains, whereas the latter level is high enough to trigger breakdown at  $Re_x \approx 2 \cdot 10^5$  in the middle of the domain.

Figures 29 and 30 display some instantaneous flow fields for the two levels of  $Tu$ . The uncontrolled (*i.e.* pure bypass transition cases) are shown as subfigures a): Streaks grow in a non-modal way throughout the boundary layer, until turbulent spots intermittently appear as isolated instabilities on individual streaks, as expected for bypass transition. The remaining cases correspond to runs in which streaks of moderate amplitude are included at the inlet of the domain. The different streak amplitudes correspond to streaks B, C and D in Table 1. If not subject to free-stream turbulence, all of these streaks would be stable. A clear trend can already now be observed: the higher the amplitude of the added streaks, the earlier the transition location.

The same conclusion can also be drawn from the evolution of the skin-friction coefficient  $c_f$  and the shape factor  $H_{12}$ , displayed in Fig. 31. The transition promotion is more relevant for lower levels of  $Tu$ , for which the natural streaks have a lower growth rate. At  $Tu = 3\%$  the transition point moves to  $Re_x = 3.5 \cdot 10^5$  compared to the uncontrolled case where turbulent spots develop only seldomly within the box (the friction coefficient  $c_f$  remains close to its laminar value). As the turbulence intensity  $Tu$  increases, the differences between the cases is less evident, but the same conclusion basically holds as it can be seen from the skin friction evolution in Fig. 31b).

The evolution of the maximum streamwise fluctuation,  $u_{\text{rms,max}}$ , shown in Figs. 31e) and f), allows an interesting interpretation of the mechanism on which the breakdown relies. This particular quantity is usually used in order to measure and represent the strength of the streamwise streaks in the boundary layer. In Fig. 31e), also the data for the cases without free-stream turbulence are displayed for reference (referred to as “undisturbed streaks”). The initial behaviour of  $u_{\text{rms,max}}$  for cases with the same streak amplitude  $A_{\text{st}}$  and with/without free-stream turbulence is very similar. As the downstream position  $Re_x$  is increased the external disturbances start to penetrate the boundary layer. Compared to the uncontrolled case, the growth of the streamwise perturbation inside the boundary layer is always larger in case of control, leading to the conclusion that external FST is mainly adding to the existing streaks in the boundary layer, causing a strengthening of the existing streaks. An opposite cancelling effect could not be observed in the averaged sense. Finally, it can be observed that the breakdown to turbulence

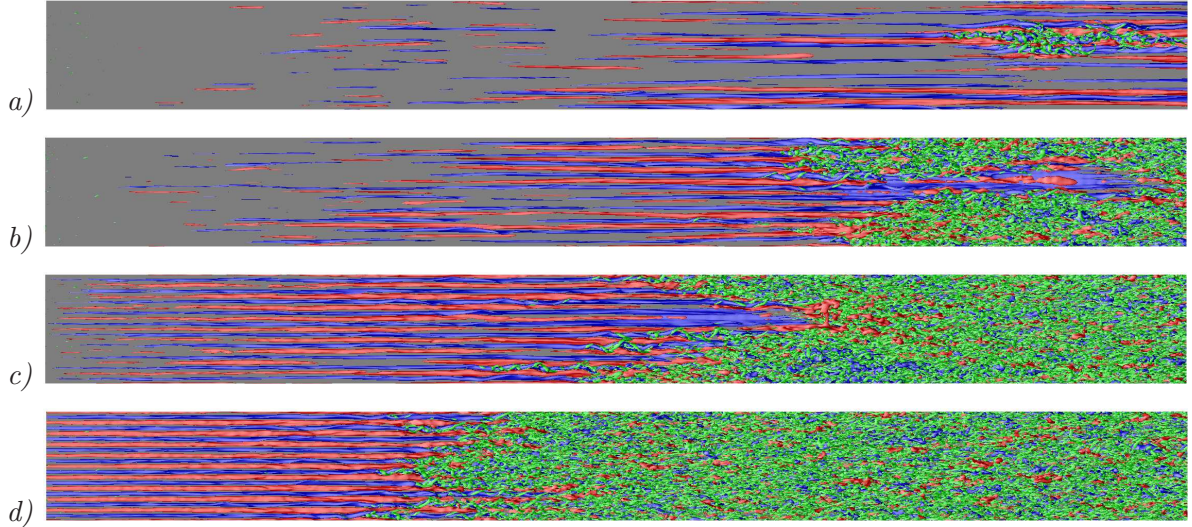


Figure 29: Top view of the three-dimensional flow structures under the influence of free-stream turbulence with  $Tu = 3.0$  as well as streaks forced in the fringe region. *a)* to *d)*: no streaks (“uncontrolled”), streak D, streak C, streak B.

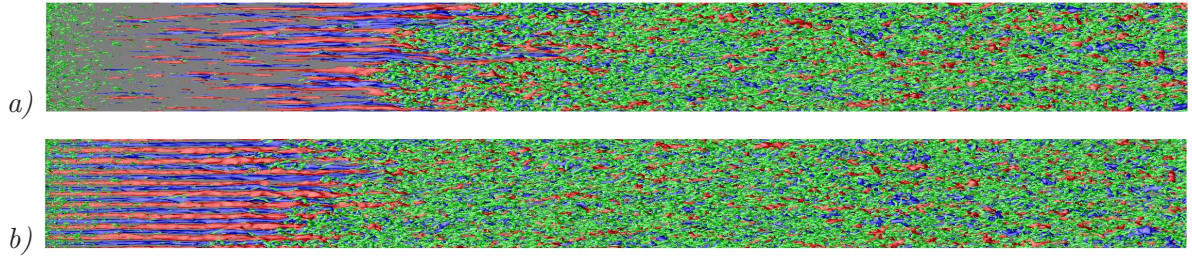


Figure 30: Top view of the three-dimensional flow structures under the influence of free-stream turbulence with  $Tu = 4.7$  as well as streaks are forced in the fringe. *a)* no streaks (“uncontrolled”), *b)* streak B.

occurs roughly at the position with the same level of  $u_{\text{rms,max}} \approx 0.15U_\infty$ .

On the other hand, a closer inspection of the instantaneous flow visualisations in Figs. 29 and 30 shows that the streaks are more straight and much longer if already introduced in the fringe region with sufficient amplitude. A blow-up of the vortical structures just prior to breakdown taken from Fig. 29*c)* is provided in Fig. 32: The growing instabilities which lead to transition in this case closely resemble the ones observed for high-amplitude streaks also found in theoretical and numerical studies [44]. The sinuous-type instability is clearly dominant, and clearly develops as a wavepacket on the streaks [48]. The varicose scenario, possibly related to the streamwise interaction of low- and high-speed streaks as proposed by de Lange and Brandt [30] would not be active in the present cases as the streak length is greatly increased.

One can thus conclude that transition to turbulence is promoted when adding streamwise streaks (*e.g.* experimentally by vortex generators or roughness elements, numerically by including them as boundary conditions) and therefore it is not a successful passive control method. As soon as the level of ambient free-stream turbulence is sufficiently high (say  $Tu > 3\%$ ), premature transition is triggered. This finding is in good agreement with the results of the earlier sections in this paper, namely those related to the oblique (three-dimensional) waves, Sec. 4 and the stochastic noise, Sec. 5. In both of these cases, the dominant instability mechanism changed

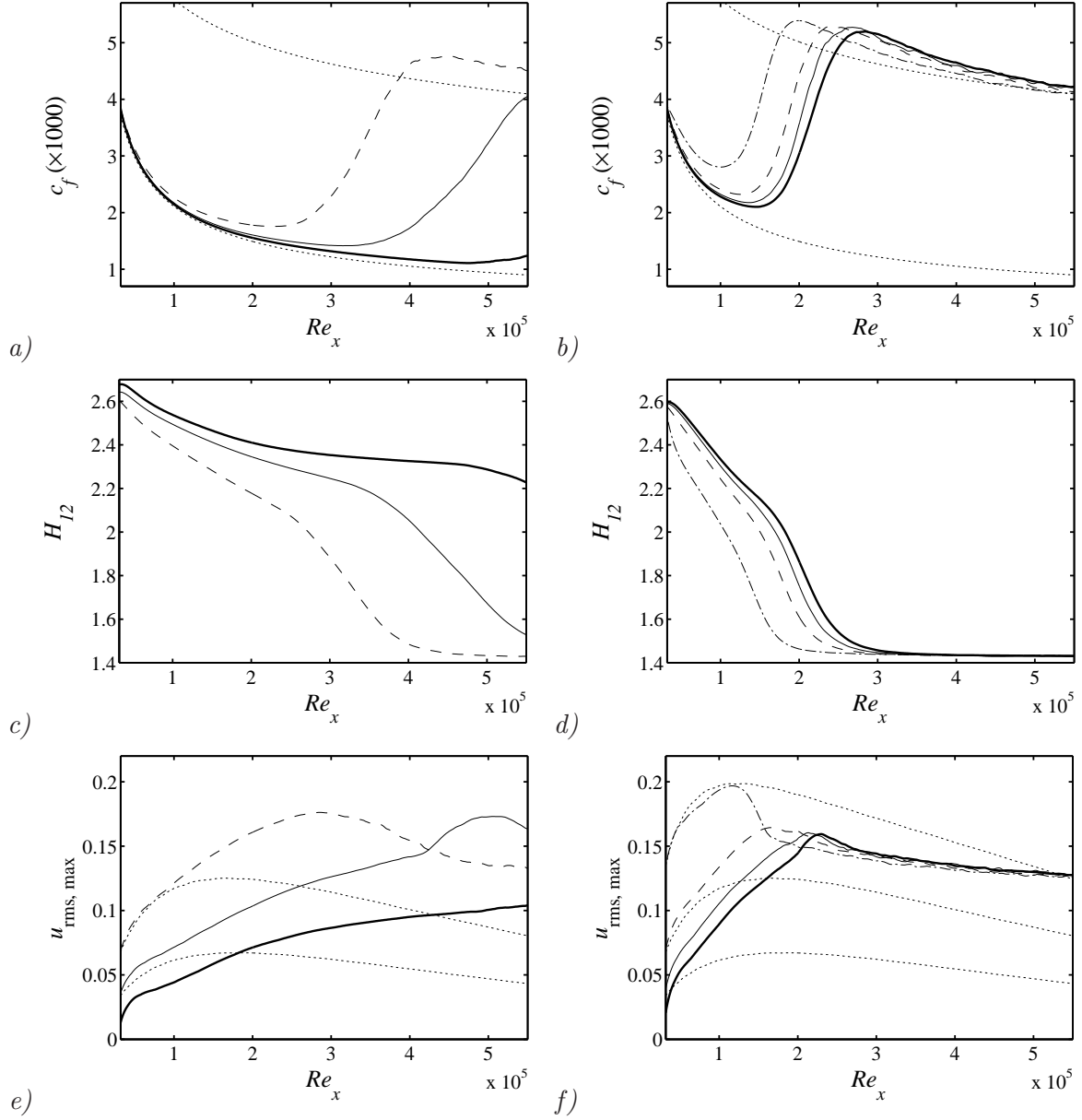


Figure 31: Transition induced by free-stream turbulence,  $Tu = 3.0\%$  (left column) and  $Tu = 4.7\%$  (right column). *Top row*: Skin friction coefficient  $c_f$ , *middle row*: Shape factor  $H_{12}$  and *bottom row*:  $u_{\text{rms,max}}$  averaged in time and spanwise direction. --- Streak B (just for  $Tu = 4.7$ ), ---- Streak C, —— Streak D, —— uncontrolled (no streak), .....  $u_{\text{rms,max}}$  for undisturbed streak.

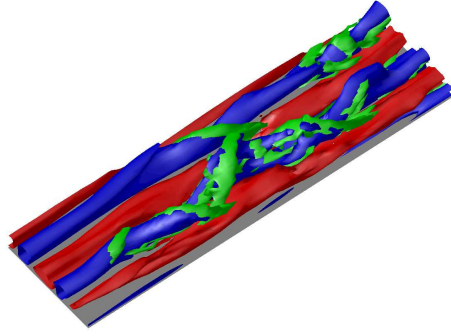


Figure 32: Instantaneous flow structure taken as a blow-up of Fig. 29*c*).

from a secondary instability of a primary TS-wave to streak instability (bypass transition) and the control approach investigated is counterproductive.

## 7 Conclusions

Passive control of the laminar-turbulent transition process in flat-plate boundary-layer flows is studied using well-resolved and well-validated large-eddy simulation (LES), based on a high-order relaxation method. The specific control mechanism consists of modifying the laminar boundary-layer profile by a spanwise periodic array of steady boundary-layer streaks. This method has been shown in theoretical [11] and experimental studies [14] as an effective way to stabilise two-dimensional Tollmien-Schlichting (TS) waves in a boundary layer. In our numerical simulations, the use of LES allowed large computational domains both in the streamwise and spanwise direction and an extensive parameter study. The streaks are forced at the inflow as optimal solutions to the linear parabolic stability equations (PSE), whereas the additional disturbances are excited via volume forcing active within the computational domain.

We examine the effect of the steady modulations on the amplification of different types of disturbances such as TS-waves, stochastic noise and free-stream turbulence. We are indeed able to confirm the stabilising effect of finite-amplitude steady streaks on the evolution of two-dimensional TS-waves. If small-amplitude random background noise of steady and unsteady nature is excited in the flow in addition to the primary TS disturbances, transition to turbulence is triggered in a natural way. However, when steady streaks are introduced upstream, transition is no more observed within our computational domain. The effect of varying the streak amplitude is analysed, and a new phenomena is outlined at low streak amplitudes (or for lower TS frequencies) where more complicated nonlinear interactions are possible. The interaction between TS-waves and streaks of comparable amplitudes leads indeed to a significant growth of oblique modes ( $\omega_0, \pm\beta_{st}$ ). This, in turn, induces a strong amplification of the steady  $(0, 2\beta_{st})$  mode, *i.e.* a doubling of the initial streaks is observed. Our results also indicate that streaks of larger spanwise scales, of the order of those of the secondary TS instability, promote the transition process: transition delay is observed for streaks of spanwise size of the order of the boundary layer thickness. Furthermore, we confirm that control by streaks can also be effective to delay transition in case of stochastic two-dimensional noise. In this case, the transition process is still dominated by the linear amplification of TS waves and therefore spanwise modulations of the boundary layer flow are an effective control approach.

The response of the boundary layer to fully three-dimensional excitations has not been considered in previous experimental studies and it is therefore analyzed here to verify the robustness of the control strategy using streaks. We demonstrate that, as soon as a significant three-dimensionality is dominant, as in *e.g.* oblique or bypass transition, control by streaks leads often to premature transition. It is finally confirmed that the streaks generated randomly in a boundary layer subject to free-stream turbulence have a damping effect on TS-waves, in agreement with experimental studies by Boiko *et al.* [23]. However, the addition of streamwise streaks cannot delay bypass transition *per se*. To summarise, control by means of streaks appear to be effective only in low-disturbance environments where boundary layer transition is initiated by the amplification of, mainly two-dimensional, TS waves. In noisy environments and in the presence of significant three-dimensional disturbances, when transition is caused by the streak secondary instability, the addition of steady spanwise modes is promoting transition. In this case, one may need to resort to opposition-control type of approach to cancel incoming high-amplitude streaks. Such an approach would however require knowledge of the flow state and a feedback loop between sensors and actuators.

Throughout the paper, various visualisations of the transitional and turbulent flow fields are used to highlight the different vortical structures and the interactions that are relevant to the different breakdown scenarios and to the control by streamwise streaks. When the flow spanwise modulation prevents laminar-turbulent transition, the occurrence of  $\Lambda$ -vortices

is observed. Conversely, the flow structures observed just prior to breakdown consist in all cases of a wavepacket traveling on the low-speed streaks; the appearance of staggered vortical structures, typical of sinuous streaks instability, is clearly documented here.

**Acknowledgments** Computer time provided by SNIC (Swedish National Infrastructure for Computing) is gratefully acknowledged.

## References

- [1] S. Bagheri, L. Brandt, and D. S. Henningson. Input-output analysis, model reduction and control of the flat-plate boundary layer. *J. Fluid Mech.*, 620:263–298, 2009.
- [2] A. Monokrousos, L. Brandt, P. Schlatter, and D. S. Henningson. DNS and LES of estimation and control of transition in boundary layers subject to free-stream turbulence. *Int. J. Heat Fluid Flow*, 29(3):841–855, 2008.
- [3] Y. Du and G. E. Karniadakis. Suppressing wall turbulence by means of a transverse travelling wave. *Science*, 288:1230–1234, 2000.
- [4] C. Viotti, M. Quadrio, and P. Luchini. Streamwise oscillations of spanwise velocity at the wall of a channel for drag reduction. *Phys. Fluids*, 21(115109), 2009.
- [5] M. Quadrio, P. Ricco, and C. Viotti. Streamwise-traveling waves of spanwise wall velocity in a turbulent channel flow. *J. Fluid Mech.*, 627:161–178, 2009.
- [6] T. Min, S. M. Kang, J. L. Speyer, and J. Kim. Sustained sub-laminar drag in a fully developed channel flow. *J. Fluid Mech.*, 558:309–318, 2006.
- [7] J. Hoepffner and K. Fukagata. Pumping or drag reduction? *J. Fluid Mech.*, 635:171–187, 2009.
- [8] T. R. Bewley. A fundamental limit on the balance of power in a transpiration-controlled channel flow. *J. Fluid Mech.*, 632:443–446, 2009.
- [9] R. Moarref and M. R. Jonavović. Controlling the onset of turbulence by streamwise traveling waves. part 1: Receptivity analysis. *J. Fluid Mech.*, 663:70–99, 2010.
- [10] C. Lee, T. Min, and J. Kim. Stability of channel flow subject to wall blowing and suction in the form of a traveling wave. *Phys. Fluids*, 20(101513), 2008.
- [11] C. Cossu and L. Brandt. Stabilization of Tollmien-Schlichting waves by finite amplitude optimal streaks in the Blasius boundary layer. *Phys. Fluids*, 14(8):L57–L60, 2002.
- [12] C. Cossu and L. Brandt. On Tollmien-Schlichting-like waves in streaky boundary layers. *Eur. J. Mech. B/Fluids*, 23:815–833, 2004.
- [13] J. H. M. Fransson, L. Brandt, A. Talamelli, and C. Cossu. Experimental study of the stabilization of Tollmien-Schlichting waves by finite amplitude streaks. *Phys. Fluids*, 17(054110):1–15, 2005.
- [14] J. H. M. Fransson, A. Talamelli, L. Brandt, and C. Cossu. Delaying transition to turbulence by a passive mechanism. *Phys. Rev. Lett.*, 96(064501):1–4, 2006.

- [15] J. H. M. Fransson, L. Brandt, A. Talamelli, and C. Cossu. Experimental and theoretical investigation of the nonmodal growth of steady streaks in a flat plate boundary layer. *Phys. Fluids*, 16(10):3627–3638, 2004.
- [16] S. Bagheri and A. Hanifi. The stabilizing effect of streaks on TS and oblique waves: A parametric study. *Phys. Fluids*, 19:078103, 2007.
- [17] P. Schlatter, H. C. de Lange, and L. Brandt. Numerical study of the stabilisation of Tollmien-Schlichting waves by finite amplitude streaks. In R. Friedrich, N. A. Adams, J. K. Eaton, J. A. C. Humphrey, N. Kasagi, and M. A. Leschziner, editors, *Turbulence and Shear Flow Phenomena 5*, pages 849–854, 2007.
- [18] I. Tani and H. Komoda. Boundary layer transition in the presence of streamwise vortices. *J. Aerospace Sci.*, 29:440, 1962.
- [19] H. Komoda. Nonlinear development of disturbance in a laminar boundary layer. *Phys. Fluids Suppl.*, 10:S87, 1967.
- [20] Y. S. Kachanov and O. I. Tararykin. Experimental investigation of a relaxing boundary layer. *Izv. SO AN SSSR, Ser. Tech. Nauk*, 18, 1987.
- [21] D. Arnal and J. C. Juillen. Contribution expérimentale à l’étude de la reptivité d’une couche limite laminaire à la turbulence de l’écoulement général. Rapport Technique 1/5018, ONERA, 1978.
- [22] H. R. Grek, V. V. Koslov, and M. P. Ramazanov. Investigation of boundary layer stability in the presence of high degree of free-stream turbulence. In *Proc. of Intl Seminar of Problems of Wind Tunnel Modeling*, volume 1, Novosibirsk (in Russian), 1989.
- [23] A. V. Boiko, K. J. A. Westin, B. G. B. Klingmann, V. V. Kozlov, and P. H. Alfredsson. Experiments in a boundary layer subjected to free stream turbulence. Part 2. The role of TS-waves in the transition process. *J. Fluid Mech.*, 281:219–245, 1994.
- [24] P. Schlatter, H. C. de Lange, and L. Brandt. The effect of free-stream turbulence on the growth and breakdown of Tollmien-Schlichting waves. In J. M. L. M. Palma and A. Silva Lopes, editors, *Advances in Turbulence XI*, pages 179–181. Springer, Berlin, Germany, 2007.
- [25] Y. Liu, T. A. Zaki, and P. A. Durbin. Boundary-layer transition by interaction of discrete and continuous modes. *J. Fluid Mech.*, 604:199–233, 2008.
- [26] Y. Liu, T. A. Zaki, and P. A. Durbin. Floquet analysis of secondary instability of boundary layers distorted by Klebanoff streaks and Tollmien-Schlichting waves. *Phys. Fluids*, 20(124102), 2008.
- [27] H. Fasel. Numerical investigation of the interaction of the Klebanoff-mode with a Tollmien-Schlichting wave. *J. Fluid Mech.*, 450:1–33, 2002.
- [28] T. Herbert. Secondary instability of boundary layers. *Annu. Rev. Fluid Mech.*, 20:487–526, 1988.
- [29] L. Brandt, P. Schlatter, and D. S. Henningson. Transition in boundary layers subject to free-stream turbulence. *J. Fluid Mech.*, 517:167–198, 2004.

- [30] L. Brandt and H. C. de Lange. Streak interactions and breakdown in boundary layer flows. *Phys. Fluids*, 20(024107):1–16, 2008.
- [31] M. T. Landahl. A note on an algebraic instability of inviscid parallel shear flows. *J. Fluid Mech.*, 98:243–251, 1980.
- [32] P. J. Schmid and D. S. Henningson. *Stability and Transition in Shear Flows*. Springer, Berlin, Germany, 2001.
- [33] M. Chevalier, P. Schlatter, A. Lundbladh, and D. S. Henningson. SIMSON - A Pseudo-Spectral Solver for Incompressible Boundary Layer Flows. Technical Report TRITA-MEK 2007:07, KTH Mechanics, Stockholm, Sweden, 2007.
- [34] J. Nordström, N. Nordin, and D. S. Henningson. The fringe region technique and the Fourier method used in the direct numerical simulation of spatially evolving viscous flows. *SIAM J. Sci. Comput.*, 20(4):1365–1393, 1999.
- [35] P. Schlatter, S. Stolz, and L. Kleiser. LES of transitional flows using the approximate deconvolution model. *Int. J. Heat Fluid Flow*, 25(3):549–558, 2004.
- [36] S. Stolz, N. A. Adams, and L. Kleiser. The approximate deconvolution model for large-eddy simulations of compressible flows and its application to shock-turbulent-boundary-layer interaction. *Phys. Fluids*, 13(10):2985–3001, 2001.
- [37] P. Schlatter, S. Stolz, and L. Kleiser. LES of spatial transition in plane channel flow. *J. Turbulence*, 7(33):1–24, 2006.
- [38] P. Schlatter, Q. Li, G. Brethouwer, A. V. Johansson, and D. S. Henningson. Simulations of spatially evolving turbulent boundary layers up to  $Re_\theta = 4300$ . *Int. J. Heat Fluid Flow*, 31:251–261, 2010.
- [39] P. Schlatter, S. Stolz, and L. Kleiser. Analysis of the SGS energy budget for deconvolution- and relaxation-based models in channel flow. In E. Lamballais, R. Friedrich, B. J. Geurts, and O. Métais, editors, *Direct and Large-Eddy Simulation VI*, pages 135–142. Springer, Dordrecht, The Netherlands, 2006.
- [40] T. Herbert. Parabolized stability equations. In *Progress in Transition Modelling*, pages 4–1–4–33. AGARD, 1993.
- [41] P. Schlatter, R. Örlü, Q. Li, G. Brethouwer, J. H. M. Fransson, A. V. Johansson, P. H. Alfredsson, and D. S. Henningson. Turbulent boundary layers up to  $Re_\theta = 2500$  studied through numerical simulation and experiments. *Phys. Fluids*, 21(051702):1–4, 2009.
- [42] P. Schlatter, Q. Li, G. Brethouwer, A. V. Johansson, and D. S. Henningson. Structure of a turbulent boundary layer studied by DNS. In *Direct and Large-Eddy Simulation 8, July 7-9 2010*, 2010. To appear.
- [43] O. Levin and D. S. Henningson. Exponential vs algebraic growth and transition prediction in boundary-layer flow. *Flow Turbulence Combust.*, 70:183–210, 2003.
- [44] P. Andersson, L. Brandt, A. Bottaro, and D. S. Henningson. On the breakdown of boundary layer streaks. *J. Fluid Mech.*, 428:29–60, 2001.
- [45] J. Jeong and F. Hussain. On the identification of a vortex. *J. Fluid Mech.*, 285:69–94, 1995.

- [46] Y. S. Kachanov. Physical mechanisms of laminar-boundary-layer transition. *Annu. Rev. Fluid Mech.*, 26:411–482, 1994.
- [47] L. Brandt and D. S. Henningson. Transition of streamwise streaks in zero-pressure-gradient boundary layers. *J. Fluid Mech.*, 472:229–261, 2002.
- [48] P. Schlatter, L. Brandt, H. C. de Lange, and D. S. Henningson. On streak breakdown in bypass transition. *Phys. Fluids*, 20(101505):1–15, 2008.
- [49] B. Rehill, E. J. Walsh, P. Schlatter, L. Brandt, K. Nolan, D. S. Henningson, and D. M. McEligot. Entropy generation rate in turbulent spots in a boundary layer subject to free stream turbulence. In P. Schlatter and D. S. Henningson, editors, *Seventh IUTAM Symposium on Laminar-Turbulent Transition*, pages 557–560. Springer, Berlin, Germany, 2010.